# A strong mitigation scenario maintains climate neutrality of northern peatlands

Chunjing Qiu, Philippe Ciais, Dan Zhu, Bertrand Guenet, Jinfeng Chang, Nitin Chaudhary, Thomas Kleinen, Xinyu Li, Jurek Müller, Yi Xi, et al.

▶ **To cite this version:**

Chunjing Qiu, Philippe Ciais, Dan Zhu, Bertrand Guenet, Jinfeng Chang, et al.. A strong mitigation scenario maintains climate neutrality of northern peatlands. One Earth, 2022, 5 (1), pp.86 - 97. 10.1016/j.oneear.2021.12.008 . hal-03607600

**HAL Id: hal-03607600**
**https://hal.science/hal-03607600**

Submitted on 14 Mar 2022

**HAL** is a multi-disciplinary open access archive for the deposit and dissemination of scientific research documents, whether they are published or not. The documents may come from teaching and research institutions in France or abroad, or from public or private research centers.

L'archive ouverte pluridisciplinaire **HAL**, est destinée au dépôt et à la diffusion de documents scientifiques de niveau recherche, publiés ou non, émanant des établissements d'enseignement et de recherche français ou étrangers, des laboratoires publics ou privés.

Distributed under a Creative Commons Attribution - NonCommercial - NoDerivatives 4.0 International License

Article

One Earth

# A strong mitigation scenario maintains climate neutrality of northern peatlands

## Graphical abstract

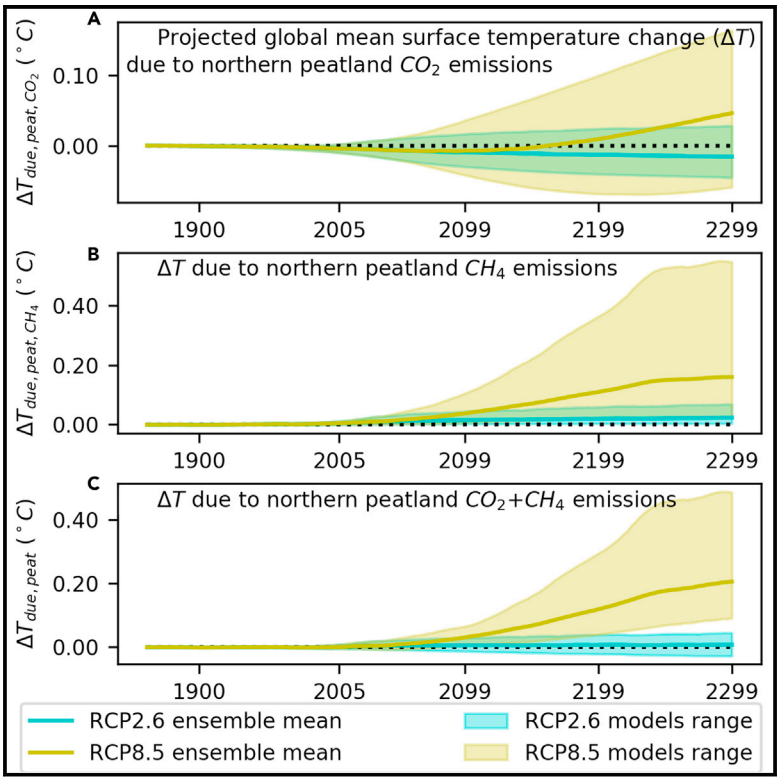


## Highlights

- Northern peatlands remain a $CO_2$ sink of ~0.1 Pg C $year^{-1}$ until 2300 under RCP2.6
- Northern peatlands become a $CO_2$ source of ~0.2 Pg C $year^{-1}$ by 2300 under RCP8.5
- $CH_4$ emissions from northern peatlands will increase 5-fold by 2300 under RCP8.5
- Modeling of peatland resilience, vegetation, and peat quality changes should be improved

## Authors

Chunjing Qiu, Philippe Ciais, Dan Zhu, ..., Narasinha J. Shurpali, David Wårlind, Sebastian Westermann

## Correspondence

chunjing.qiu@lsce.ipsl.fr

## In brief

Northern peatlands are one of the biggest terrestrial carbon pools, yet their response to climate change is uncertain. This study uses five state-of-the-art peatland models to project future $CO_2$ and $CH_4$ fluxes. Northern peatlands are projected to be climate neutral under a climate mitigation scenario consistent with the Paris Agreement goals, but they release $CO_2$ and $CH_4$ in the long term for high warming scenarios, exacerbating global warming by 0.21°C. The results suggest that climate mitigation efforts will prevent northern peatlands from amplifying climate warming.

Qiu et al., 2022, One Earth 5, 86–97
January 21, 2022 © 2021 The Authors. Published by Elsevier Inc.
https://doi.org/10.1016/j.oneear.2021.12.008

CellPress

CellPress
OPEN ACCESS

Gold Standard for the Global Goals
3 tons of $CO_2$ offset

One Earth

Article

# A strong mitigation scenario maintains climate neutrality of northern peatlands

Chunjing Qiu,[1,2,25,*] Philippe Ciais,[1] Dan Zhu,[1,3] Bertrand Guenet,[1,4] Jinfeng Chang,[5] Nitin Chaudhary,[6,10] Thomas Kleinen,[7] XinYu Li,[3] Jurek Müller,[8,9] Yi Xi,[3] Wenxin Zhang,[10,11] Ashley Ballantyne,[12] Simon C. Brewer,[13] Victor Brovkin,[7] Dan J. Charman,[14] Adrian Gustafson,[10] Angela V. Gallego-Sala,[14] Thomas Gasser,[15] Joseph Holden,[16] Fortunat Joos,[8,9] Min Jung Kwon,[1] Ronny Lauerwald,[17] Paul A. Miller,[10] Shushi Peng,[3] Susan Page,[18] Benjamin Smith,[10,19] Benjamin D. Stocker,[20,21] A. Britta K. Sannel,[22] Elodie Salmon,[1,23] Guy Schurgers,[11] Narasinha J. Shurpali,[24] David Wårlind,[10] and Sebastian Westermann[6]

[1]Laboratoire des Sciences du Climat et de l'Environnement, UMR8212, CEA-CNRS-UVSQ, 91191 Gif-sur-Yvette, France
[2]Université Paris-Saclay, INRAE, AgroParisTech, UMR MIA 518, 75231 Paris, France
[3]Sino-French Institute for Earth System Science, College of Urban and Environmental Sciences, Peking University, 100871 Beijing, China
[4]Laboratoire de Géologie, UMR 8538, Ecole Normale Supérieure, PSL Research University, CNRS, Paris, France
[5]College of Environmental and Resource Sciences, Zhejiang University, Hangzhou, 310058, China
[6]Department of Geosciences, University of Oslo, 0371 Oslo, Norway
[7]Max Planck Institute for Meteorology, 20146 Hamburg, Germany
[8]Climate and Environmental Physics, Physics Institute, University of Bern, 3012 Bern, Switzerland
[9]Oeschger Center for Climate Change Research, University of Bern, 3012 Bern, Switzerland
[10]Department of Physical Geography and Ecosystem Science, Lund University, 22362 Lund, Sweden
[11]Center for Permafrost (CENPERM), Department of Geosciences and Natural Resource Management, University of Copenhagen, Copenhagen, Denmark
[12]Department of Ecosystem and Conservation Science, University of Montana, Missoula, MT 59801, USA
[13]Department of Geography, University of Utah, Salt Lake City, UT, USA
[14]Geography Department, College of Life and Environmental Sciences, University of Exeter, Exeter, EX4 4RJ, UK
[15]International Institute for Applied Systems Analysis (IIASA), 2361 Laxenburg, Austria
[16]School of Geography, University of Leeds, Leeds LS2 9JT, UK
[17]Université Paris-Saclay, INRAE, AgroParisTech, UMR ECOSYS, 78850 Thiverval-Grignon, France
[18]School of Geography, Geology and the Environment, University of Leicester, Leicester, UK
[19]Hawkesbury Institute for the Environment, Western Sydney University, Richmond, NSW, Australia
[20]Department of Environmental Systems Science, ETH Zürich, 8092 Zürich, Switzerland
[21]Swiss Federal Institute for Forest, Snow and Landscape Research WSL, Birmensdorf, Switzerland
[22]Department of Physical Geography, Stockholm University, 106 91 Stockholm, Sweden
[23]Laboratoire de Physique et Chimie de l'Environnement et de l'Espace, LPC2E, 45071 Orléans cedex 2, France
[24]Natural Resources Institute Finland, Production Systems, Halolantie 31 A, 71750 Maaninka, Finland
[25]Lead contact
*Correspondence: chunjing.qiu@lsce.ipsl.fr
https://doi.org/10.1016/j.oneear.2021.12.008

**SCIENCE FOR SOCIETY** Intact peatlands remove carbon dioxide ($CO_2$) from the atmosphere through photosynthesis and store the carbon in soils in waterlogged conditions, while emitting methane ($CH_4$) to the atmosphere. The net climate impact of peatlands depends on the relative magnitude of these two greenhouse gases. Here, we assess the future $CO_2$ and $CH_4$ balance of northern peatlands using five large-scale, process-based peatland models. Our results suggest that under climate policies and action, northern peatlands are likely be climate neutral because the climate-warming effect of peatland $CH_4$ emissions is offset by the cooling effect of peatland $CO_2$ sinks. However, if action on climate change is not taken, northern peatlands could accelerate global warming because $CH_4$ emissions are projected to increase substantially, and northern peatlands may turn from $CO_2$ sinks to sources driven by strong warming and drying.

## SUMMARY

Northern peatlands store 300–600 Pg C, of which approximately half are underlain by permafrost. Climate warming and, in some regions, soil drying from enhanced evaporation are progressively threatening this large carbon stock. Here, we assess future $CO_2$ and $CH_4$ fluxes from northern peatlands using five land surface models that explicitly include representation of peatland processes. Under Representative Concentration Pathways (RCP) 2.6, northern peatlands are projected to remain a net sink of $CO_2$ and climate neutral for

 © 2021 The Authors. Published by Elsevier Inc.
This is an open access article under the CC BY-NC-ND license (http://creativecommons.org/licenses/by-nc-nd/4.0/).

the next three centuries. A shift to a net $CO_2$ source and a substantial increase in $CH_4$ emissions are projected under RCP8.5, which could exacerbate global warming by 0.21°C (range, 0.09–0.49°C) by the year 2300. The true warming impact of peatlands might be higher owing to processes not simulated by the models and direct anthropogenic disturbance. Our study highlights the importance of understanding how future warming might trigger high carbon losses from northern peatlands.

## INTRODUCTION

Global mean surface temperatures are projected to increase by 0.3–4.8°C (relative to 1986–2005) by the end of the 21st century.[1] Unabated greenhouse gas (GHG) emissions, such as those of carbon dioxide ($CO_2$) and methane ($CH_4$) in the RCP8.5 scenario and its extension (see experimental procedures), may result in a 3.0–12.6°C global mean warming by the year 2300.[1] Given that warming is amplified in the northern mid- and high latitudes compared with the global average,[2] the stability of soil organic carbon (SOC) stocks of northern peatlands (300–600 Pg C)[3–5] is of particular concern.

The future carbon balance of northern peatlands remains, however, poorly understood, with only a few studies attempting a quantification for the 21st century[6–13]; even less work has been done on predicting peatland carbon fluxes beyond 2100.[8–10,14,15] Using evidence from the literature and expert elicitation, Loisel et al.[14] found that peatland experts anticipate peat carbon gains in northern regions owing to higher temperatures and peat carbon losses as a result of permafrost degradation through to the year 2300. Gallego-Sala et al.[15] examined relationships between peat carbon accumulation rates of the last millennium and different climate parameters; they found a positive relationship between peat carbon accumulation rates and growing-season cumulative photosynthetically active radiation (PAR) for northern peatlands. They predicted that northern peatlands would remain a carbon sink until 2300 under both RCP2.6 and RCP8.5 scenarios, with the carbon sink capacity of Arctic peatlands predicted to increase continuously while that of temperate peatlands is predicted to decrease. However, projected future warming is much greater and faster than changes in the last millennium[1,16] and may be accompanied by more frequent and severe droughts.[17] With drastic anticipated changes in temperatures and hydroclimate (particularly the water-table position, which is one of the most important controls on peatland carbon balance), peatlands may be pushed beyond their natural envelope, and the abiotic factors that appear to have been correlated with peat carbon accumulation rates in the last millennium cannot be expected to remain the dominant controls in the future.[18–20]

Process-based models, which explicitly parameterize peatland hydrological, thermal, and biogeochemical processes, can account for the complex interactions among factors that are important in driving the dynamics of peatland ecosystems (e.g., temperature, soil moisture, vegetation type, thaw depth, $CO_2$ fertilization). They are useful tools to explore responses of peatlands to future climate changes. Yet, peatlands are not explicitly represented in the land surface of the current generation of earth system models (ESMs), and only a few studies have considered peatland carbon-climate feedbacks using coupled peatland-climate models.[9] Previous studies based on independent offline peatland model simulations have already provided some insight into the future carbon balance of peatlands. However, it is difficult to draw robust conclusions because critical inputs (i.e., climate forcing, peatland extent, peat initiation time) were different among simulations resulting in divergent projections.[7,8,11–13] In addition, while most previous attempts considered only changes in the rates of peatland carbon accumulation/storage or focused only on $CO_2$ fluxes,[7,8,11–15] the relative contribution of different GHGs (i.e., $CO_2$ versus $CH_4$) is essential information if we are to understand the influence of peatlands on the global carbon cycle and on the Earth's climate system.[9] Furthermore, a timescale of the next century is too short to look at if we want to elucidate the full peatland responses to warming, owing to long (decades to centuries) lags in the response of slow-turnover peatland carbon pools to climate forcing.[8]

To address the above research gaps, we conducted a multi-model assessment of changes of net $CO_2$ and $CH_4$ fluxes from intact northern peatlands (north of 30°N latitude) using state-of-the-art large-scale peatland models, ORCHIDEE-PEAT,[21,22] LPJ-MPI,[23] LPX-Bern,[8,13,24–27] LPJ-GUESS,[28,29] and LPJ-GUESS_dynP ("dynP" for dynamic multi-peat layers)[11,12,30] (see Note S1 and Tables S1–S3 for more detailed information about each model). The models were forced with a fixed peatland extent (Figure 1)[31] and integrated from 10,000 years before the present to the year 2300 following a common simulation protocol (see experimental procedures). The same atmospheric $CO_2$ concentration and bias-corrected gridded climate projections from the IPSL-CM5A-LR general circulation model (GCM)[32] for a strong climate mitigation scenario (RCP2.6) and a high-end emission scenario (RCP8.5) were used to drive all models. The global mean warming over land under RCP2.6 is projected to reach 1.6°C (1.9°C over land >30°N) by 2100 relative to 1986–2005 in the IPSL-CM5A-LR GCM, followed by a steady but small cooling trend until 2300. In contrast, a dramatic global land warming is projected for RCP8.5, with the air temperature increasing by ~5.9°C (6.7°C over land >30°N) by 2100 and ~14.7°C by 2300 (15.5°C over land >30°N) (see Figure S1).

## RESULTS AND DISCUSSION

### Projected carbon dioxide budget of northern peatlands

Simulated present-day (1986–2005) total SOC stock for the 3.2 million $km^2$ covered by northern peatlands[31] ranges from 200 to 870 Pg C among models (Figure S2), which brackets previous estimates based on observations (300–600 Pg C).[3–5] The multi-model ensemble mean SOC (572 Pg C) falls close to the mean from observations. Hereafter, we report multi-model ensemble mean values, with ranges across models in parentheses, unless stated otherwise.

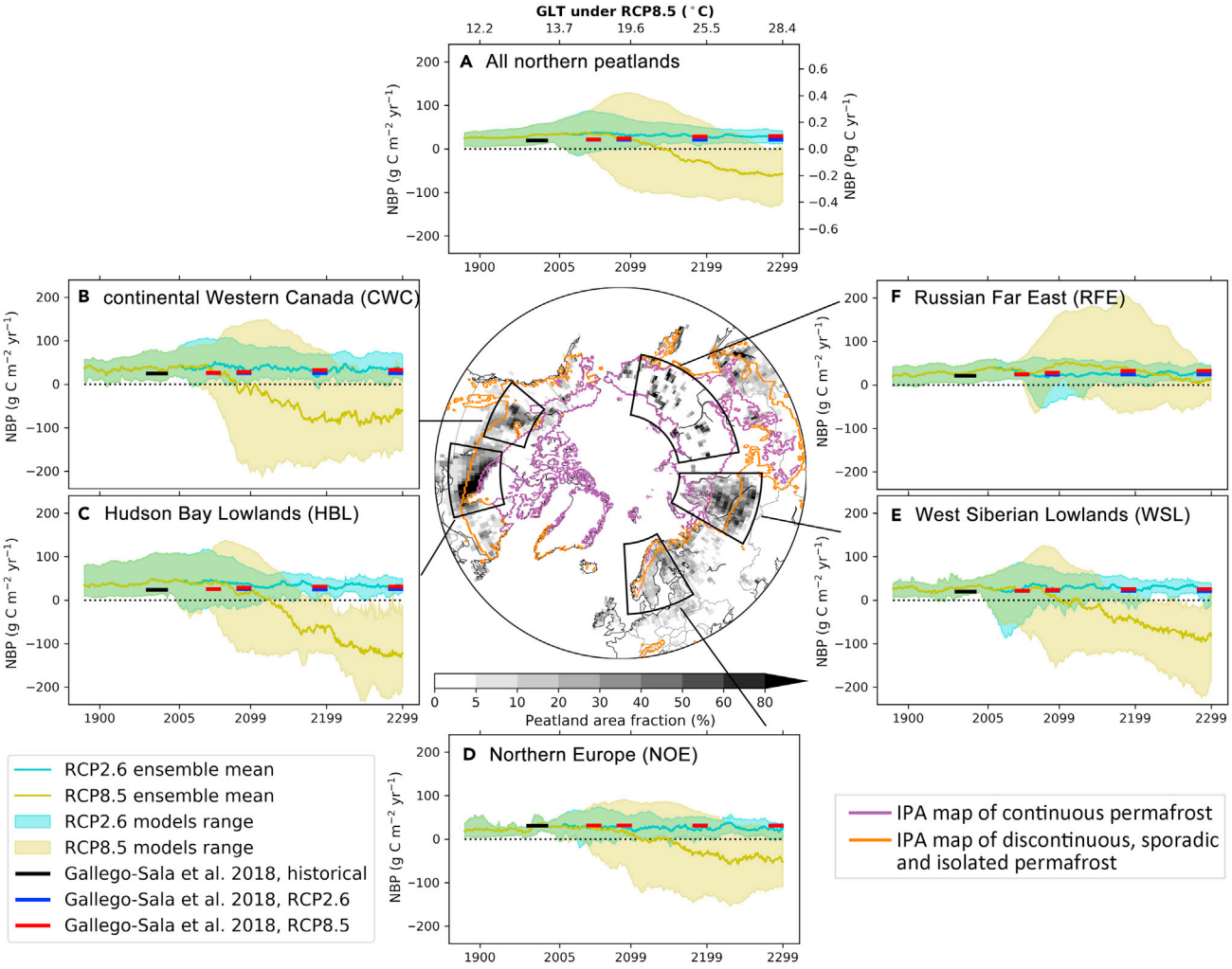


**Figure 1. Projected northern peatland NBP under RCP2.6 and RCP8.5**

(A–F) Simulated time series (range and ensemble mean) of area-averaged peatland NBP under RCP2.6 (cyan) and RCP8.5 (yellow) by all five models participating in this study (a positive sign represents $CO_2$ fluxes from the atmosphere to the peatland ecosystem) and predicted carbon sequestration by peat accumulated during the last millennium estimated by Gallego-Sala et al.[15] The central map shows peatland areal fractions from PEATMAP[31]; the extent of continuous permafrost and discontinuous, sporadic, and isolated permafrost are from the empirical IPA (International Permafrost Association) permafrost map.[33] Peatland NBP values shown in this figure are 20-year moving averages, and moving average values were assigned to the last year of each window period. The 20-year moving averages of the surface air temperature over global land (GLT) from the IPSL-CM5A-LR GCM under RCP8.5 are shown in (A).

The $CO_2$ balance of peatlands in this study, termed the net biome production (NBP), is calculated as net primary productivity (NPP) minus heterotrophic respiration—anthropogenic disturbances of peatland and fires are not modeled. A positive NBP thus represents a $CO_2$ flux from the atmosphere to the land. Simulated present-day NBP of all northern peatlands is 0.11 (0.01–0.22) Pg C year$^{-1}$ (Figure 1A), matching previous estimates for the Northern Hemisphere (0.10–0.15 Pg C year$^{-1}$).[5,15,34] The projected future NBP of northern peatlands depends on the trajectory of climate change. Under RCP2.6, northern peatlands remain $CO_2$ sinks with a relatively stable net $CO_2$ uptake rate until 2300 (Figure 1A). By contrast, under RCP8.5, northern peatlands turn into a $CO_2$ source within the coming 100–150 years (Figure 1A). The simulated future carbon balance of peatlands varies among subregions in response to projected strong climate warming and precipitation changes in RCP8.5. For four subregions out of the five main peat complexes of the Northern Hemisphere, i.e., continental Western Canada (CWC) (Figure 1B), Hudson Bay Lowlands (HBL) (Figure 1C), Northern Europe (NOE) (Figure 1D), and West Siberian Lowlands (WSL) (Figure 1E), all models projected a future shift from peatland $CO_2$ sinks to $CO_2$ sources (or to nearly carbon neutral) under RCP8.5. Two models (LPX-Bern and LPJ-GUESS), which explicitly simulated coupled peatland nitrogen and carbon cycling, projected that these peatlands will be larger $CO_2$ sources in the future, as opposed to models in which NPP is not limited by available soil nitrogen (ORCHIDEE, LPJ-MPI and LPJ-GUESS_dynP). For the Russian Far East (RFE) (Figure 1F), where the projected increase in precipitation is the largest under RCP8.5 (110% increase in RFE precipitation by 2300 with

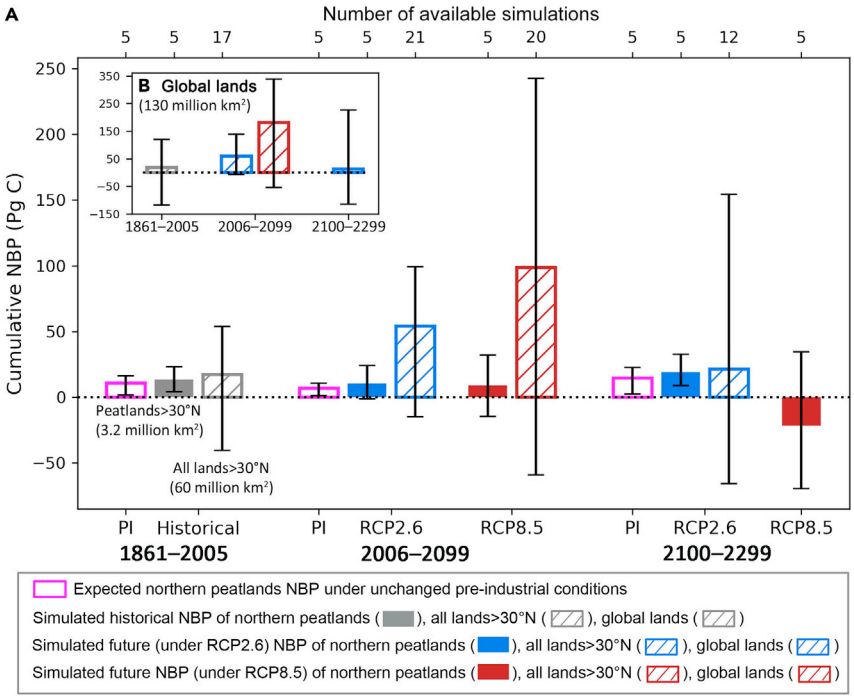


**Figure 2. Simulated cumulative NBP of northern peatlands compared with that of all lands**

(A) Simulated cumulative NBP of northern peatlands (filled bars) from this study and simulated cumulative NBP of all lands north of 30°N (hatched bars) from ISIMIP2b[32] for 1861–2005 (gray bars) and for the future RCP2.6 (blue bars) and RCP8.5 (red bars) scenarios. Open magenta bars show expected northern peatland $CO_2$ fluxes under unchanged pre-industrial (PI) conditions. A positive NBP represents $CO_2$ fluxes from the atmosphere to the land. The number of available simulations for each period is indicated by the top x axis (Table S4). The black error bars indicate the full range across simulations. (B) The inset (B) shows cumulative NBP of the global lands from ISIMIP2b. Note that peatlands have not been explicitly represented in ISIMIP2b models, but carbon fluxes due to historical land use change have been accounted for, with future land use being held constant at 2005 levels. ISIMIP2b models were driven only up to the year 2099 for the RCP8.5 scenario.

respect to present-day versus 5%–75% increase in precipitation for the other four subregions) (Figure S1), only one model (LPJ-GUESS) predicts that this peatland complex will become a large net source of $CO_2$ in the future. All five models project a trend toward shallower water tables for RFE peatlands (Figure S3), indicating that RFE peat remains preserved by anoxic conditions below the water table.

Simulated NBP of peatlands for all five subregions is in good agreement with the empirical extrapolation of peat accumulation made by Gallego-Sala et al.[15] under RCP2.6. However, under RCP8.5, only the simulated NBP of RFE peatlands, where the largest increase in precipitation and persistent anoxic conditions is projected, is comparable to the estimate from Gallego-Sala et al.[15] For the other four subregions (CWC, HBL, NOE, and WSL), Gallego-Sala et al. predicted a slight increase of peatland NBP under RCP8.5, in contrast to the mechanistic models applied here. Gallego-Sala et al. considered only peat that accumulated during the last millennium and ignored the decomposition of deeper (older) peat. When the water table drops below a critical level, as projected by some of our models (Figure S3), the exposure of deeper peat to aerobic and warmer conditions results in substantial loss of carbon.[18,35,36]

There is a large variation in the simulated trajectories of peatland carbon dynamics under RCP8.5 among model simulations. This variation is due to substantial differences among models in the parameterization of peatland vegetation, hydrological and thermal processes (Note S1 and Tables S1 and S2) and consequently a wide range of predicted peatland water balance terms (Figures S3 and S4), soil temperature (Figure S5), NPP (Figure S6), and carbon inputs to the soil in these simulations.

Figures S7–S9 show the capability of the models to reproduce the current water-table position and NBP at the site level. Peatland development is strongly governed by local conditions, and it is therefore nearly impossible for large-scale models to exactly reproduce the development of peatland at each site. LPJ-GUESS and LPJ-GUESS_dynP better captured the interannual, among-sites variability in peatland water-table position. However, because the projected RCP8.5 climate lies far outside of past conditions for which we can validate the models, there is no way to ascertain which one of the models simulates the peatland hydrological and carbon dynamics most accurately under the extreme and long-term warming coupled to elevated $CO_2$ concentrations of RCP8.5.

## Northern peatlands in the global carbon cycle

To quantify the role of northern peatlands in the global carbon cycle, in this study we compare the NBP of northern peatlands with the NBP of all other northern (>30°N) and global lands (Figure 2). Estimates for NBP of all northern and global lands from land surface model (LSM) simulations are from the Inter-Sectoral Impact Model Intercomparison Project (ISIMIP2b; https://doi.org/10.5880/PIK.2019.012),[32] in which peatlands have not been explicitly represented, but carbon fluxes due to land-use changes have been accounted for. Six ISIMIP2b LSMs were forced by bias-corrected climate forcing data from four different GCMs, with all simulations for the RCP8.5 scenario driven only up to the year 2099, and some simulations for the RCP2.6 scenario extended to 2300 (Table S4).

We show that despite a large spread between individual models, the simulated cumulative NBP of northern peatlands is of the same order of magnitude as the NBP of the entire northern or global land biosphere (Figure 2), although northern peatlands cover only ~2% of the global land area. Over 2006–2099, the ISIMIP2b models project that the northern and global land biosphere $CO_2$ sink is larger under RCP8.5 than under RCP2.6. This difference is attributable to vegetation $CO_2$ uptake by photosynthesis being favored by very high $CO_2$ levels in RCP8.5.[37] In contrast, our peatland models simulate a smaller

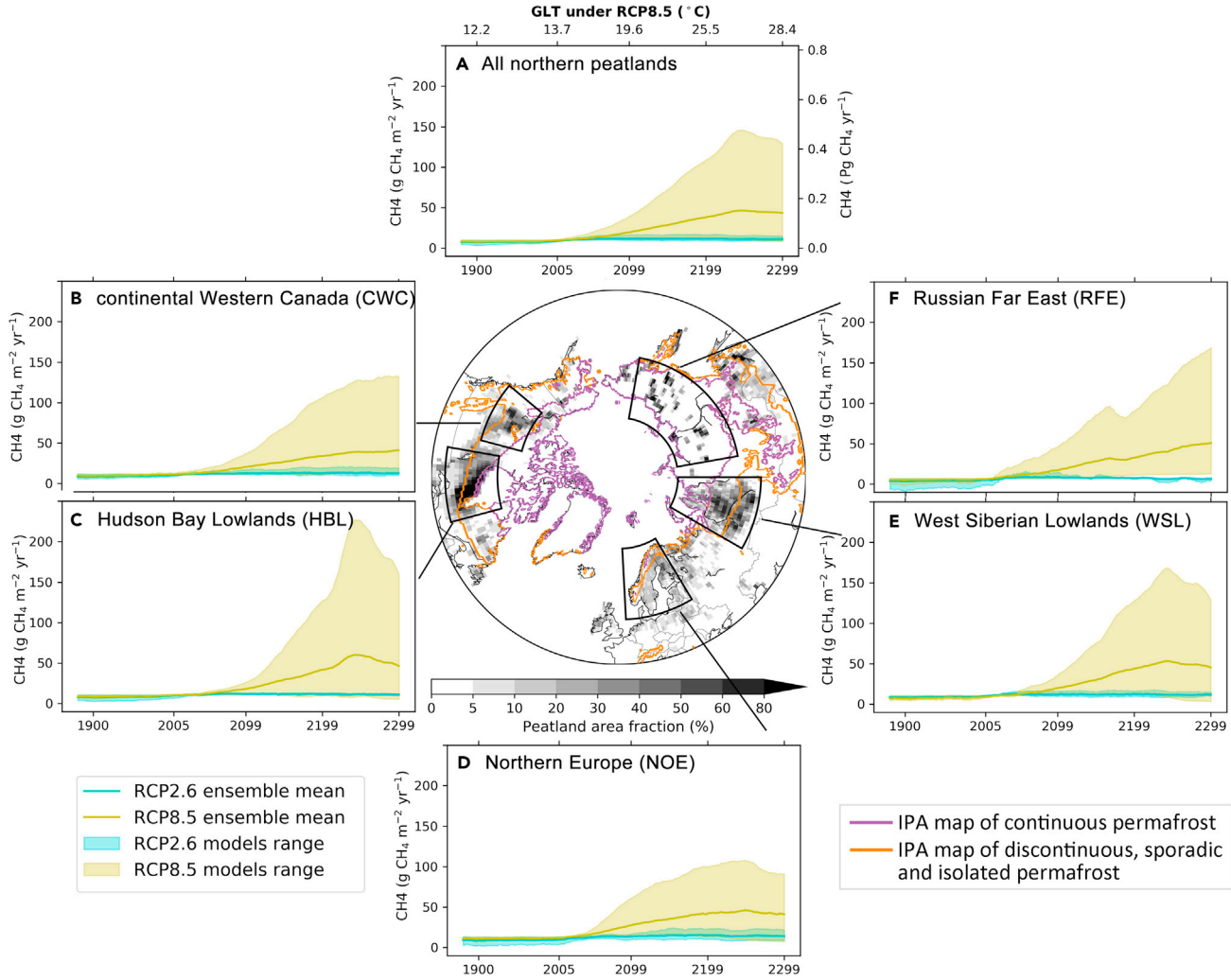


**Figure 3. Projected northern peatland $CH_4$ emissions under RCP2.6 and RCP8.5**

(A–F) Same as Figure 1, but for area-averaged rates of bias-corrected $CH_4$ emissions from northern peatlands.

$CO_2$ sink over northern peatlands in RCP8.5 than in RCP2.6. Over 2100–2300, northern peatlands are projected to remain $CO_2$ sinks under RCP2.6, with their cumulative NBP amounting to 19 (9–32) Pg C. In contrast, the mean cumulative NBP of northern peatlands under RCP8.5 is −21 (−69 to 34) Pg C, with four out of five models predicting a net loss of carbon by peatlands over 2100–2300.

## Projected methane emissions from northern peatlands

Rising $CH_4$ emissions from peatlands have a warming impact on the climate system and thus need to be considered when calculating the net radiative balance of peatlands.[34] Simulated present-day $CH_4$ emissions from northern peatlands range from 5 to 87 Tg $CH_4$ $year^{-1}$. Compared with observation-based estimates at the site level,[38] LPJ-GUESS_dynP overestimates peatland $CH_4$ emissions, while the other models underestimate them (Figure S10). We applied an absolute-trend-preserving gridcell by gridcell bias correction (see experimental procedures) based on a gridded data product of northern wetland methane emissions.[39] After applying this bias correction, simulated peatland $CH_4$ emissions at the site level show better agreement with observations (i.e., bias and root-mean-squared difference between simulated and observed $CH_4$ were reduced) (Figure S10), and bias-corrected present-day $CH_4$ emissions from all northern peatlands are 26–32 Tg $CH_4$ $year^{-1}$.

In the future, $CH_4$ emissions from northern peatlands are projected to remain relatively stable until 2300 under RCP2.6 according to the ensemble mean (Figure 3A). Under RCP8.5, the wide range of simulated NPP and/or SOC (defining the substrate for $CH_4$ production), soil moisture and temperature result in a large variation in the simulated rates of $CH_4$ emissions among models. LPX-Bern and LPJ-GUESS, which couple carbon and nitrogen cycles, project an initial increase of $CH_4$ emissions, followed by a decrease until 2300 owing to the limited availability of substrate for methanogenesis (i.e., both models predicted a decrease of NPP after 2200) and the deepening of peatland water tables under RCP8.5. In contrast, the other three models project a continuous increase in northern peatland $CH_4$ emissions under RCP8.5 until

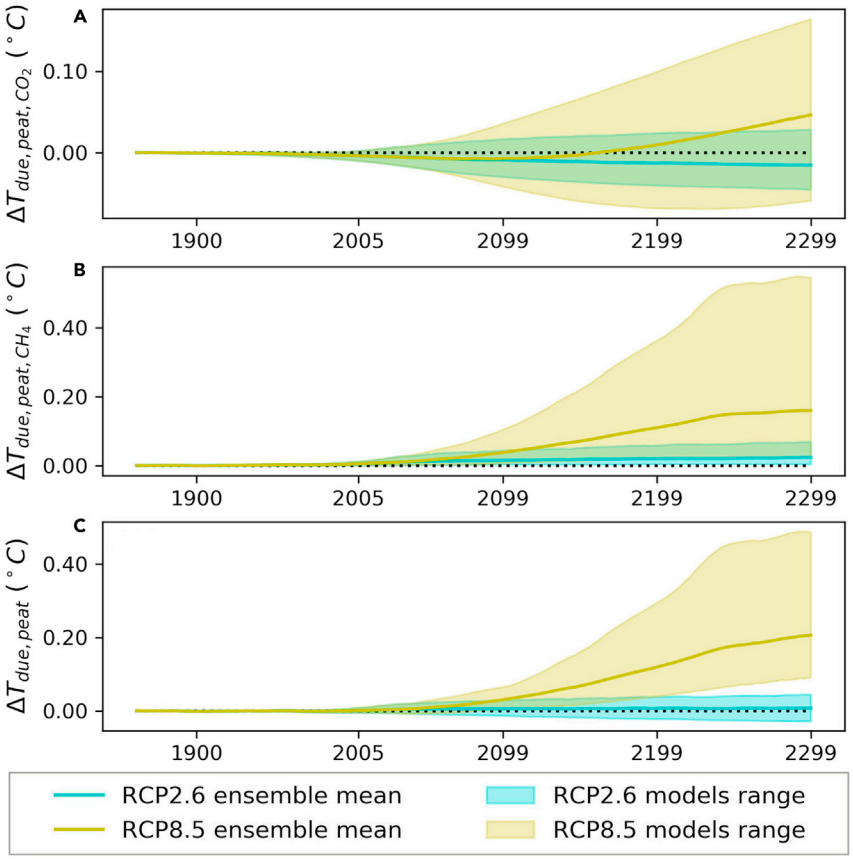


**Figure 4. Projected global mean surface temperature change (ΔT) due to northern peatland anthropogenic GHG emissions**

(A–C) ΔT due to northern peatland anthropogenic $CO_2$ emissions (A), ΔT due to northern peatland anthropogenic $CH_4$ emissions (B), and ΔT due to total GHG ($CO_2$+$CH_4$) emissions (C), under RCP2.6 (cyan) and RCP8.5 (yellow), relative to pre-industrial times.

2300, as the projected drop of water tables is smaller and/or the projected amount of substrate for methanogenesis is more stable (i.e., projected NPP is relatively stable in the future).

Simulated trajectories of peatland $CH_4$ emissions under RCP8.5 differ among peatland regions (Figures 3B–3F). $CH_4$ emissions from CWC and RFE peatlands are projected to increase until 2300, while a decrease of $CH_4$ emissions in the second half of the 23rd century is projected for peatlands in HBL, NOE, and WSL. This can be attributed to changes in substrate availability and water-table depth among regions, i.e., both NPP and water-table depth of RFE peatlands remain stable after 2250, and thus RFE $CH_4$ emissions are projected to increase with increasing temperature. Water-table depths of HBL peatlands also remain generally stable, but simulated NPP is projected to decrease because the projected increase in plant respiration continues to increase faster than gross primary productivity (Figure S11); thus, HBL $CH_4$ emissions are projected to decrease after 2250.

## Projected net climate effect of northern peatlands

During pre-industrial times, northern peatlands sequestered $CO_2$ and emitted $CH_4$, while the global climate was relatively stable.[1] Thus, only the difference between simulated northern peatland GHG fluxes presented in previous sections and pre-industrial fluxes represents the net climate change effect of northern peatlands. Following Cain et al.,[40] we approximated the impact of a step change in peatland $CH_4$ emissions on the global average surface temperature with a pulse emission of $CO_2$ (experimental procedures). Figure 4 shows the simulated global mean surface temperature change (ΔT) due to changes of northern peatland $CO_2$ and $CH_4$ fluxes from the pre-industrial values. Under RCP2.6, northern peatlands are projected to exert a small cooling effect on global climate through $CO_2$ sequestration, with the multi-model mean ΔT of −0.02 (−0.05 to +0.03) °C by 2300 (Figure 4A). A small warming effect on global climate is projected owing to northern peatland $CH_4$ emissions, with the multi-model mean of +0.02 (+0 to +0.07) °C by 2300 (Figure 4B). Therefore, northern peatlands are projected to be climate neutral under RCP2.6 (−0.03 to +0.05°C by 2300), when both $CO_2$ and $CH_4$ are accounted for (Figure 4C). In contrast, under RCP8.5, the global mean surface temperature change caused by northern peatlands by 2300 is projected to be 0.21 (+0.09 to +0.49) °C higher than the pre-industrial value, with a warming of +0.16 (+0.02 to +0.55) °C attributable to northern peatland $CH_4$ emissions and a warming of +0.05 (−0.06 to +0.16) °C attributable to northern peatland $CO_2$ emissions.

## Permafrost peatlands versus non-permafrost peatlands

Nearly half of the present-day northern peatland area and peat SOC pool are affected by permafrost (Figure 1), making the carbon relatively inert.[5] However, rapid warming such as under RCP8.5 could lead to permafrost thaw and release of GHGs into the atmosphere.[41,42] To compare the simulated GHG emissions of permafrost versus non-permafrost peatlands, we define permafrost peatlands as those underlain by continuous/discontinuous/sporadic permafrost according to the empirical International Permafrost Association (IPA) permafrost map[33] (experimental procedures). The total area of permafrost peatlands is ~1.4 million $km^2$, accounting for ~44% of the northern peatland area. Note that the permafrost soils may have changing active layer thickness, and permafrost may disappear as a result of future warming (Figure S12). Yet, the IPA permafrost area was applied for the past and the future in the following analysis, and thus changes over time for the same area are assessed.

Models project slightly larger $CO_2$ sequestration rates (in g C per unit area of peatland per year) for permafrost than for non-permafrost peatlands during the periods of 1861–1880 and 1986–2005 (Figure 5). In the future under RCP8.5, with large uncertainties, a slower decrease in $CO_2$ sequestration rates of permafrost compared with non-permafrost peatlands is

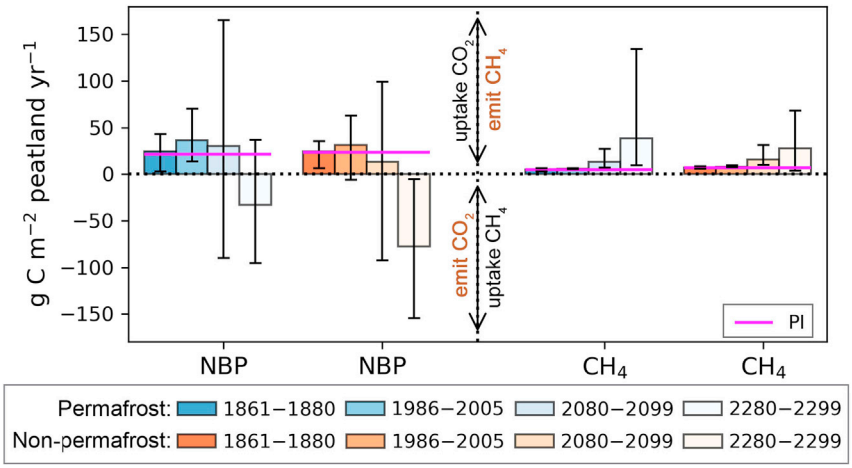


**Figure 5. Projected GHG fluxes from regions covered today by permafrost and non-permafrost peatlands under RCP8.5**

$CO_2$ and $CH_4$ from regions covered today by permafrost (blue) and non-permafrost (orange) peatlands under RCP8.5 are averaged over 1861–1880, 1986–2005, 2080–2099, and 2280–2299. Positive values of $CO_2$ represent sinks, that is, $CO_2$ fluxes from the atmosphere to the peatland ecosystem, while positive values of $CH_4$ represent $CH_4$ fluxes from the peatland ecosystem to the atmosphere. Black error bars indicate the full range across simulations. Magenta lines show expected fluxes (ensemble mean) under unchanged pre-industrial (PI) conditions (ranges across models shown in Figure S14). Note that water-ice phase change, and thus permafrost, was not represented in LPJ-MPI. Therefore, this figure shows only data from the other four models.

projected, and permafrost peatlands are projected to turn into smaller $CO_2$ sources than non-permafrost ones by 2280–2300. The simulated rates of $CH_4$ emissions in permafrost peatlands are slightly lower than in non-permafrost peatlands during the periods of 1861–1880 and 1986–2005 (in g C per unit area of peatland per year). However, permafrost peatlands are projected to become larger $CH_4$ sources than non-permafrost peatlands by 2280–2300. For both permafrost and non-permafrost peatlands, the relative contribution of $CH_4$ to the full GHG balance is projected to increase over time.

These results must be interpreted with care, however. The first reason is the uncertainty related to the extent of permafrost peatlands. The extent of permafrost peatlands is determined from the observation-based IPA permafrost map and was fixed from 1861 to 2300. Owing to differences in model structure, simulated soil temperature and active layer thickness (ALT) differ substantially between models (Figures S12 and S13). Simulated current ALT by some models was larger than 6 m for some permafrost peatlands, meaning that all SOC of those peatlands is already within the active layer today, while the true ALT in permafrost peatlands is generally much thinner (Figure S13). The second reason for taking care in interpreting our results is that permafrost peatlands are dominated by ice-rich landforms—so-called peat plateaus and palsas—for which rapid thaw pathways due to thermokarst exist.[43,44] Thermokarst not only affects the timing and speed of thawing, but also has a strong impact on the temperature and moisture conditions after thawing and thus on the direction and magnitude of permafrost-carbon feedback to climate.[42] For land-surface schemes, model approaches for thermokarst in peatlands are in an early, experimental stage,[45] so they are not yet included in the models employed for this study.

## Limitations to simulating the fate of peatland carbon

First, our results are drawn from only five peatland models, and only four of those models can explicitly simulate permafrost processes. To reduce uncertainty in model projections, a better understanding of the differences among models (i.e., the five models used in this study and models with a specific representation for peatland hydrology[46–49]) is needed, and our intercomparison of the five state-of-the-art peatland models represents the first step. Further work involving site-level simulations and comparison with manipulative experiments in the field are also needed. To estimate the fate of carbon in peatlands more reliably and to assess the full array of carbon-climate feedback processes, it is critical to explicitly represent the unique hydrothermal characteristics of peatlands and permafrost in the next generation of LSMs. Second, our models have been tuned and evaluated against past/contemporary climate conditions, while the projected RCP8.5 climate falls far outside the envelope of past conditions. Theoretically, models simulating the effects of the dramatic climate change under RCP8.5 could be validated against field manipulation experiments. However, manipulation experiments for peatland ecosystems are scarce, with most of them involving only a single variable during a short experimental period. The magnitudes of the increases in temperature/atmospheric $CO_2$ concentrations applied in these experiments are commonly much lower than those in RCP8.5.[50,51] Furthermore, we applied climate outputs from only a single ESM, thereby neglecting uncertainties in climate projections, which are shown to lead to large differences in projected peat carbon fluxes.[8] IPSL-CM5A-LR is the only ISIMIP2b GCM that provided climate outputs beyond 2100 for RCP8.5. The climate sensitivity of IPSL-CM5A-LR is larger than other Coupled Model Intercomparison Project Phase 5 (CMIP5) model simulations and is at the upper end of the observational range.[52,53] Additional work is required to further assess the variation in model outputs arising from the choice of climate forcing.[8] We focused on the response of peatlands to prescribed climate change in this study; however, peatland carbon-climate feedbacks should be taken into account in a fully coupled model setup in future work.

Another limitation of our modeling framework is that both peatland area and peat carbon developed dynamically after the last deglaciation and under evolving climate and $CO_2$ concentrations,[3,26] leading to large legacy effects for future peat distribution and carbon fluxes,[8] while the state of pre-industrial peatlands was modeled here by a simplistic model spin up using constant climate conditions and a fixed distribution of peatlands. Moreover, the areal extent of peatlands was fixed over the entire period of 1861–2300, and the possible expansions/contractions of peatland due to climate change and ensuing carbon sequestrations/emissions were not accounted for in this study. Yet, a

large turnover of peatland area with disappearing and newly established peatlands is found in simulations that include dynamic areas of peatland and carbon evolution.[7,8,26] Additionally, while we considered only intact peatlands, simulating GHG emissions from degraded peatlands owing to anthropogenic disturbances (e.g., drainage, rewetting, and agricultural uses) and natural and anthropogenic fires would be necessary to provide a complete picture of northern peatland GHG budgets.[34,54] Finally, tropical peatlands are increasingly recognized for their carbon stocks and GHG fluxes, but these are not yet included in most of the LSMs used here and thus in this study.[55]

Peatlands are unique, complex ecosystems that are important for the global carbon cycle.[56] Some of their unique characteristics and processes are just beginning to be implemented into LSMs and warrant further development, including, but not limited to, the following:

(1) *Vegetation dynamics:* the current representation of peatland vegetation in the models is rather simple, with one plant functional type (PFT) representing *Sphagnum* moss and another PFT representing graminoids (Table S1). Only LPJ-GUESS_dynP included five peatland PFTs, representing moss, graminoid, high deciduous shrub, low deciduous shrub, and low evergreen shrub. While growing evidence suggests that the shrubification of peatlands is regulated by climate, geomorphic, and biogeographic settings on both regional and local scales,[57,58] representing sub-grid scale conditions remains a challenge for large-scale LSMs. Of the five models, only LPJ-GUESS_dynP considered the micro-topographical structure of peatland. The patterned surface of peatland is represented by uneven heights of connected individual patches by LPJ-GUESS_dynP (five patches in each grid cell in this study), and water is redistributed from higher elevated patches to lower patches through lateral flow.[30] This will affect the vegetation composition, with mosses and graminoids thriving in moist patches, whereas shrubs are favored in dry patches. Besides the vegetation composition, the response of peatland plants to abiotic factors (such as warming, water stress, and elevated atmospheric $CO_2$) also affects peatland carbon balances. However, scarce observations often show inconclusive, contradictory results for *Sphagnum* mosses.[59,60] More field measurements/experiments and better understanding of peatland plant response to different abiotic factors are needed to improve and calibrate peatland vegetation processes in models.

(2) *Peatland resilience to drying:* the resilience of peatland to climate change is enhanced by a hydrological self-regulation mechanism; that is, a decline in hydraulic conductivity and porosity of peat due to lowering of the water table and enhanced decomposition may prevent further water loss from the peatland and lead to slower decomposition.[61,62] Of the five models, LPJ-GUESS_dynP considered the changes in peat physical (i.e., bulk density and porosity) and hydraulic (i.e., the permeability of peat layers) properties due to decomposition and compaction processes[30], while ORCHIDEE-PEAT parameterized a reduction of hydraulic conductivity with depth, but ignored its temporal variability.[21]

(3) *Changes in peat quality:* it is well known that peat quality is an important control on the mineralization of peat carbon.[63] On one hand, vegetation species composition determines the chemical composition and degradability of peat soil organic matter. On the other hand, for a given peat layer, the recalcitrant proportion of peat increases with time, as the labile fraction gets decomposed. The former mechanism is captured by four models (except for ORCHIDEE-PEAT, in which mixed plant species in northern peatlands are represented by one PFT), while the latter is considered only by ORCHIDEE-PEAT and LPJ-GUESS_dynP. In LPJ-GUESS_dynP, a new layer of peat is deposited over previously accumulated peat layers each year, and the model keeps track of these layer components as they decompose through time; each layer component becomes more recalcitrant as it becomes older.[30] In ORCHIDEE-PEAT, soil carbon is divided into three pools according to their residence time (active, slow, and passive pools), and peat becomes more recalcitrant with depth because carbon in the active pool depletes faster and feeds the slow and passive pools.

## Conclusions

In this study, we assessed past and future GHG ($CO_2$ and $CH_4$) balances of intact northern peatlands using five large-scale peatland models. The models suggest that northern peatlands will continue to remove atmospheric $CO_2$ under the relatively low-warming trajectory of RCP2.6, whereas they will become net emitters of $CO_2$ in the long-term under the high-warming trajectory of RCP8.5. In addition, a substantial increase of $CH_4$ emissions from northern peatlands is projected under RCP8.5 by all models. Northern peatlands are projected to be climate neutral until the year 2300 under RCP2.6. In contrast, under RCP8.5, $CO_2$ and $CH_4$ emissions by northern peatlands could exacerbate global warming by 0.21°C (0.09–0.49°C) by 2300. Our results demonstrate that effective mitigation policies, in particular, reduction of $CO_2$ emissions from fossil fuel burning and land use, are needed to maintain the northern peatland net atmospheric $CO_2$ sink and limit its future $CH_4$ emissions.

## EXPERIMENTAL PROCEDURES

### Resource availability

#### *Lead contact*

Further information and requests for resources should be directed to and will be fulfilled by the lead contact, Chunjing Qiu (chunjing.qiu@lsce.ipsl.fr).

#### *Materials availability*

Not applicable to this study.

#### *Data and code availability*

All input data used for the study are openly available, as stated in the article. All data generated in this study are publicly available at: https://doi.org/10.5281/zenodo.5595768. The source code for participating models will be made available on request.

### Participating models

Participating models that explicitly resolve peat carbon cycling include one LSM (ORCHIDEE-PEAT[21,22]) and four dynamic vegetation-ecosystem models (DGVMs) (LPJ-MPI,[23] LPX-Bern,[8,13,24–27] LPJ-GUESS,[28,29] and LPJ-GUESS_dynP[11,12,30]). Although all the DGVMs can be traced to the original LPJ model,[64] they have largely independent development histories and exhibit

substantial differences in structure, assumptions, and processes represented (Note S1 and Tables S1–S3).

### Simulation protocol

To maximize inter-comparability among models, all models were driven by the same meteorological forcing data (bias-corrected, daily climate fields of the IPSL-CM5A-LR GCM from ISIMIP2b[32]), atmospheric $CO_2$ concentrations,[65] and fixed peatland extent (PEATMAP from Xu et al.[31]) and followed a common simulation protocol. The four protocol steps are described as follows: (1) All models were first spun up for 10,000 years, with atmospheric $CO_2$ concentration fixed at the pre-industrial levels (286 ppm). The actual historical initiation and expansion of peatlands were asynchronous in the Northern Hemisphere, i.e., rapid expansion of Alaskan peatlands occurred in the early Holocene, while the highest rate of peatland formation in the Hudson Bay Lowlands (HBL) occurred in the mid-Holocene.[66,67] As northern peatlands showed a peak initiation around 10 ka in most regions,[67,68] we spun up all models over 10,000 years in this study to approximate peat carbon accumulation during the Holocene. Repeated 1961–1990 meteorological forcing was used in this step to approximate the Holocene temperatures, which were higher than pre-industrial levels.[16] (2) All models were run for another 100 years with repeated 1901–1920 meteorological forcing to adjust simulated soil hydrological and thermal variables and carbon fluxes to pre-industrial conditions. (3) A historical simulation was conducted from 1861 to 2005, with historical meteorological forcing from IPSL-CM5A-LR GCM and historical rising atmospheric $CO_2$ concentration. (4) Two final future simulations were undertaken from 2006 to 2300, driven by RCP2.6 and RCP8.5 scenarios and their extensions and with RCP-driven climate outputs of the IPSL-CM5A-LR GCM. LPJ-MPI conducted simulations at 0.5° × 0.5° spatial resolution, while the other models conducted simulations at 1° × 1° spatial resolution.

### RCP2.6 and RCP8.5 scenarios and their extensions

The RCP2.6 scenario represents a strong mitigation scenario with the radiative forcing (RF) peaking at ~3 W $m^{-2}$ before 2100 and then declining to 2.6 W $m^{-2}$ by 2100. RCP2.6 is extended to 2300, assuming constant emissions after 2100.[65] The RCP8.5 scenario represents a very high emission scenario, in which RF rises to 8.5 W $m^{-2}$ by 2100. Beyond 2100, following a stylized emission trajectory, the RF under RCP8.5 further increases to 12 W $m^{-2}$ by 2250 and then stabilizes at 12 W $m^{-2}$ until 2300.

### Bias correction of simulated peatland $CH_4$ emissions

The gridded wetland $CH_4$ emissions (using the PEATMAP distribution map) during 2013 and 2014 from Peltola et al.[39] derived by upscaling eddy-covariance $CH_4$ measurements are used as reference observations (*Obs*) for the bias correction of models. Our bias correction aims at correcting present-day emissions to realistic values, while it preserves model predictions of future and past changes. Simulated $CH_4$ emissions south of 45°N were not corrected because *Obs* covers only regions north of 45°N, but this has little effect on the estimate of northern peatland $CH_4$ emissions given that only ~0.2 million $km^2$ of northern peatlands are in the regions south of 45°N.

We apply the spatial bias correction method from Pulliainen et al.[69] For each grid cell and from each model, we first calculate the bias in simulated $CH_4$:

$$Bias_{i,j} = \frac{1}{2}\left(\left(Sim_{i,j}^{2013} - Obs_i^{2013}\right) + \left(Sim_{i,j}^{2014} - Obs_i^{2014}\right)\right) \quad \text{(Equation 1)}$$

where $Sim_{i,j}^{2013}$ and $Sim_{i,j}^{2014}$ are simulated $CH_4$ emissions for grid cell $i$ by model $j$, in the years 2013 and 2014, respectively; and $Obs_i^{2013}$ and $Obs_i^{2014}$ are observed $CH_4$ emissions[39] counterparts.

Then, assuming that the bias remains temporally constant, the simulated $CH_4$ of each grid cell is bias-corrected:

$$corrected\ Sim_{i,j}^{t} = Sim_{i,j}^{t} - Bias_{i,j} \quad \text{(Equation 2)}$$

where $Sim_{i,j}^{t}$ is the simulated $CH_4$ emission for grid cell $i$ by model $j$ and in the year $t$, with $t$ varying from 1861 to 2300.

### Calculation of the net climate effect of northern peatlands

The conventional Global Warming Potential (GWP) emission metric has been widely used to compare different climate forcers. Emissions of a given climate forcer ($E$) is converted to $CO_2$-equivalent emissions ($E_{CO2-e}$) by multiplying it by a GWP factor over a specified time horizon ($H$):

$$E_{CO_2-e} = E \times GWP_H \quad \text{(Equation 3)}$$

where $GWP_H$ is the conventional GWP for the given forcer over the specified time horizon $H$. However, GWP cannot represent the effect of gas emissions on temperature.[40,70,71] Emissions of a long-lived climate forcer (LLCF) add cumulatively into the atmosphere and result in an increase of air temperature as long as emissions are maintained, i.e., a linear relationship has been found between global mean temperature increase and cumulative $CO_2$ emission—the transient climate response to cumulative $CO_2$ emissions (TCRE).[1] The resultant warming would persist for centuries even if the emission of $CO_2$ had stopped.[72] For short-lived climate forcers (SLCF) (i.e., $CH_4$), if emissions are maintained at a constant rate, the atmospheric $CH_4$ concentration will be stabilized after the emissions are balanced by natural atmospheric removals.[73] Thus, constant $CH_4$ emissions will result in stable forcing and no additional temperature increases. If $CH_4$ emissions were to decrease or stop, atmospheric $CH_4$ concentration would decrease and result in cooling. The GWP (Equation 3), however, would incorrectly suggest that decreases in $CH_4$ emissions will cause further warming.

To consistently express emissions of short- and long-lived forces and their climate impacts, a new usage of GWP, denoted GWP*, was proposed by Allen et al.[70] and refined by Cain et al.[40] Allen et al.[70] equated a change in the emission rate of a given short-lived forcer ($\Delta E_{SLCF}$) to a one-off pulse emission or sequestration of $\Delta E_{SLCF} \times H \times GWP_H$ of $CO_2$ (denoted $CO_2$-e*) and then refined GWP* by spreading the pulse emission over $\Delta t$ years following the change in the SLCF emission rate, thus reducing the volatility of $E_{CO2-e*}$ and better representing the effect of SLCF on temperature:

$$E_{CO_2-e*} = GWP_H \times \frac{\Delta E_{SLCF}}{\Delta t} \times H \quad \text{(Equation 4)}$$

To take into account the delayed response of temperature to past changes in the SLCF emission rate, Cain et al.[40] redefined GWP* by incorporating a "stock" term ($E_{SLCF} \times GWP_H$) into the equation of Allen et al.[70] to represent the slow adjustment of temperature to past changes in the SLCF emission rate. Using the revised definition of GWP*, the calculated $CO_2$ equivalent quantity is better associated with temperature change contribution[40,71] and is denoted $CO_2$-warming-equivalent ($CO_2$-we) in the following:

$$E_{CO_2-we} = GWP_H \times \left(r \times \frac{\Delta E_{SLCF}}{\Delta t} \times H + s \times E_{SLCF}\right) \quad \text{(Equation 5)}$$

where $\Delta E_{SLCF}$ is the change in the emission rate of the SLCF over the preceding $\Delta t$ years, $E_{SLCF}$ is the SLCF emission rate for the year under consideration, $r$ and $s$ are the weights given to the impact of changing the SLCF emission rate and the impact of the SLCF stock. The values of $r$ and $s$ are scenario dependent, as they depend on the historical trajectory of emissions and carbon cycle feedbacks. Here, we use $r = 0.68$ and $s = 0.32$ for RCP2.6 and $r = 0.73$ and $s = 0.27$ for RCP8.5,[40] with $H = 100$ years and a $GWP_{100}$ value of 28 for $CH_4$ in both scenarios.

It should be noted that northern peatlands were already a part of the global carbon cycle and the climate system in the pre-industrial era, as natural sources of $CH_4$ and sinks of $CO_2$. Given that both GHG fluxes from northern peatlands in the pre-industrial era do not contribute to the global RF, we calculate perturbed or anthropogenic $CO_2$ and $CH_4$ fluxes by subtracting simulated pre-industrial fluxes from simulated fluxes during 1861–2300. We estimated $CO_2$-we emissions from anthropogenic $CH_4$ fluxes with Equation 5. We assume that during a few hundred years before 1861, in the pre-industrial era, both $CH_4$ and $CO_2$ fluxes from northern peatlands were relatively stable and use simulated rates averaged over 1861–1870 as an approximation (magenta bars in Figure 2 and magenta lines in Figure 5).

We then calculate cumulative anthropogenic $CO_2$-we emissions from northern peatlands, which can be multiplied by the TCRE to estimate the global temperature change ($\Delta T$) due to northern peatland $CO_2$ and $CH_4$ emissions:

$$\Delta T_{due,peat,CO_2} = TCRE \times \left(\sum_{i=1861}^{2300}\left(E_{CO_2,i} - E_{CO_2,pre}\right)\right) \quad \text{(Equation 6)}$$

$$\Delta T_{due,peat,CH_4} = TCRE \times \left( \sum_{i=1861}^{2300} \left( E_{CO_2-we,i} - E_{CO_2-we,pre} \right) \right) \quad \text{(Equation 7)}$$

where $E_{CO2,i}$ and $E_{CO2,pre}$ are $CO_2$ emission rates from northern peatlands in the year $i$ and in the pre-industrial era, respectively; $E_{CO2-we,i}$ and $E_{CO2-we,pre}$ are $CO_2$-we (calculated with Equation 5) due to northern peatland $CH_4$ emissions in the year $i$ and in the pre-industrial era, respectively. TCRE is likely in the range of 0.2–0.7°C per 1,000 Pg $CO_2$ and can be assumed to be constant over time until temperatures peak.[1,74] A value of 0.4°C per 1,000 Pg $CO_2$, which is the best estimate of observationally constrained TCRE,[75] is used in this study. It should be noted that peatland ecosystems were not represented by ESMs used for estimation of TCRE.[75] One study that explicitly considered peat carbon feedbacks in their observationally constrained simulations estimated TCRE of 0.5 (68% confidence range: 0.35–0.74) °C per 1,000 Pg $CO_2$.[76] Further investigation is needed to refine the estimate by including peatland carbon-climate feedbacks in ESMs.

### Distribution of permafrost peatlands does not change with time

The distributions of permafrost peatlands could be delineated directly from the simulation of each model. However, the definitions of permafrost differ among models.[12,77] Furthermore, models do not simulate sub-grid-scale permafrost distribution, but represent the entire grid cell as either in a permafrost or in a non-permafrost state at a coarse spatial resolution of 1° × 1°. In reality, only part of a grid cell might be permafrost, such as those parts with discontinuous permafrost areas. Therefore, in this study we define permafrost peatlands as those underlain by continuous/discontinuous/sporadic permafrost according to the empirical IPA permafrost map,[33] and the areal extent of permafrost peatlands do not change with time.

## SUPPLEMENTAL INFORMATION

Supplemental information can be found online at https://doi.org/10.1016/j.oneear.2021.12.008.

## ACKNOWLEDGMENTS

This work was supported by the European Research Council Synergy grant (SyG-2013-610028 IMBALANCE-P) and the French State Aid managed by the ANR under the "Investissements d'avenir" programme (ANR-16-CONV-0003_Cland). ORCHIDEE-PEAT performed simulations using HPC resources from GENCI-TGCC (2020-A0070106328). A.V.G.-S. was funded by the Natural Environment Research Council (NERC standard grant no. NE/I012915/1 and no. NE/S001166/1). W.Z. acknowledges funding from the Swedish Research Council FORMAS 2016-01201 and Swedish National Space Agency 209/19. N.C. acknowledges funding by the Nunataryuk (EU grant agreement no. 773421) and the Swedish Research Council FORMAS (contract no. 2019-01151). LPJ-GUESS_dyn simulations were performed on the supercomputing facilities at the University of Oslo, Norway, and on the Aurora and Tetralith resources of the Swedish National Infrastructure for Computing (SNIC) at the Lund University Centre for Scientific and Technical Computing (Lunarc), project no. 2021/2-61 and no. 2021/2-28, and Linköping University, project no. snic2020/5-563. A.G., P.A.M., W.Z., B.S., D.W., and N.C. acknowledge support from the strategic research areas Modeling the Regional and Global Earth System (MERGE) and Biodiversity and Ecosystem Services in a Changing Climate (BECC) at Lund University. P.A.M. and D.W. received financial support from the H2020 CRESCENDO project (grant agreement no. 641816). LPJ-GUESS simulations were enabled by resources provided by the Swedish National Infrastructure for Computing (SNIC) at LUNARC partially funded by the Swedish Research Council through grant agreement no. 2018-05973. J.M. and F.J. acknowledge financial support by the Swiss National Science Foundation (no. 200020_172476 and no. 200020_200511) and funding from the European Union's Horizon 2020 research and innovation program under grant agreement no. 820989 (project COMFORT) and no. 821003 (project 4C). The work reflects only the authors' views; the European Commission and their executive agency are not responsible for any use that may be made of the information the work contains. B.G. received funding from the European Union's Horizon 2020 research and innovation program under grant agreement no. 641816 (CRESCENDO) and no. 821003 (4C project). B.D.S was funded by the Swiss National Science Foundation grant no. PCEFP2_181115. T.K. acknowledges support from the German Federal Ministry for Education and Research (BMBF) through the PalMod programme (grant no. 01LP1507B and no. 01LP1921A). LPJ-MPI experiments were performed at the German Climate Computing Centre (DKRZ), using resources from the Max Planck Institute for Meteorology. N.J.S. acknowledges financial support from Academy of Finland (no. 296887 and no. 334422) and the Finnish Ministry of Agriculture and Forestry (no. VN/28562/2020). J.C. acknowledged support from the Fundamental Research Funds for the Central Universities (no. 2021QNA6005). D.Z. acknowledges funding from the National Natural Science Foundation of China (grant no. 42101090 and no. 41988101). W.Z and G.S. acknowledge support from the Danish National Research Foundation (DNRF100).

## AUTHOR CONTRIBUTIONS

C.Q., P.C., D.Z., and B.G. designed the research; C.Q. and P.C. drafted the manuscript; J.C. prepared the climate forcing for ORCHIDEE-PEAT and computed estimates of global and Northern Hemisphere $CO_2$ emissions from ISIMIP2b terrestrial biosphere models; C.Q., N.C., T.K., X.Y.L., J.M., Y.X., and W.Z. performed model simulations; A.V.G.-S. and S.C.B. provided estimates for future peat carbon sink from Gallego-Sala et al.[15]; all authors contributed to the interpretation of the results and draft revision.

## DECLARATION OF INTERESTS

The authors declare no competing interests.

Received: July 23, 2021
Revised: November 1, 2021
Accepted: December 14, 2021
Published: January 6, 2022

## REFERENCES

1. IPCC (2013). Climate Change 2013. The Physical Science Basis. Working Group I Contribution to the Fifth Assessment Report of the Intergovernmental Panel on Climate Change (Cambridge University Press).
2. Seneviratne, S.I., Donat, M.G., Pitman, A.J., Knutti, R., and Wilby, R.L. (2016). Allowable $CO_2$ emissions based on regional and impact-related climate targets. Nature *529*, 477–483.
3. Yu, Z., Loisel, J., Brosseau, D.P., Beilman, D.W., and Hunt, S.J. (2010). Global peatland dynamics since the last glacial maximum. Geophys. Res. Lett. *37*, 1–5.
4. Yu, Z. (2012). Northern peatland carbon stocks and dynamics: a review. Biogeosciences *9*, 4071–4085.
5. Hugelius, G., Loisel, J., Chadburn, S., Jackson, R.B., Jones, M.C., MacDonald, G.M., Marushchak, M.E., Olefeldt, D., Packalen, M., Siewert, M.B., et al. (2020). Large stocks of peatland carbon and nitrogen are vulnerable to permafrost thaw. Proc. Natl. Acad. Sci. U S A *117*, 20438–20446.
6. Leifeld, J., Wüst-Galley, C., and Page, S. (2019). Intact and managed peatland soils as a source and sink of GHGs from 1850 to 2100. Nat. Clim. Change *9*, 945–947.
7. Qiu, C., Zhu, D., Ciais, P., Guenet, B., and Peng, S. (2020). The role of northern peatlands in the global carbon cycle for the 21st century. Glob. Ecol. Biogeogr. *29*, 956–973.
8. Müller, J., and Joos, F. (2021). Committed and projected future changes in global peatlands-continued transient model simulations since the last glacial maximum. Biogeosciences *18*, 3657–3687.
9. Stocker, B.D., Roth, R., Joos, F., Spahni, R., Steinacher, M., Zaehle, S., Bouwman, L., and Prentice, I.C. (2013). Multiple greenhouse-gas feedbacks from the land biosphere under future climate change scenarios. Nat. Clim. Change *3*, 666–672.

10. Alexandrov, G.A., Brovkin, V.A., Kleinen, T., and Yu, Z. (2020). The capacity of northern peatlands for long-term carbon sequestration. Biogeosciences *17*, 47–54.

11. Chaudhary, N., Miller, P.A., and Smith, B. (2017). Modelling past, present and future peatland carbon accumulation across the pan-Arctic region. Biogeosciences *14*, 4023.

12. Chaudhary, N., Westermann, S., Lamba, S., Shurpali, N., Sannel, A.B.K., Schurgers, G., Miller, P.A., and Smith, B. (2020). Modelling past and future peatland carbon dynamics across the pan-Arctic. Glob. Change Biol *26*, 4119–4133.

13. Spahni, R., Joos, F., Stocker, B.D., Steinacher, M., and Yu, Z.C. (2013). Transient simulations of the carbon and nitrogen dynamics in northern peatlands: from the Last Glacial Maximum to the 21st century. Clim. Past *9*, 1287–1308.

14. Loisel, J., Gallego-Sala, A., Amesbury, M., Magnan, G., Anshari, G., Beilman, D., Benavides, J., Blewett, J., Camill, P., Charman, D., et al. (2020). Expert assessment of future vulnerability of the global peatland carbon sink. Nat. Clim. Change *11*, 70–77.

15. Gallego-Sala, A.V., Charman, D.J., Brewer, S., Page, S.E., Prentice, I.C., Friedlingstein, P., Moreton, S., Amesbury, M.J., Beilman, D.W., Björck, S., et al. (2018). Latitudinal limits to the predicted increase of the peatland carbon sink with warming. Nat. Clim. Change *8*, 907–913.

16. Marcott, S.A., Shakun, J.D., Clark, P.U., and Mix, A.C. (2013). A reconstruction of regional and global temperature for the past 11,300 years. Science *339*, 1198–1201.

17. Dai, A. (2013). Increasing drought under global warming in observations and models. Nat. Clim. Change *3*, 52–58.

18. Evans, C.D., Peacock, M., Baird, A.J., Artz, R.R.E., Burden, A., Callaghan, N., Chapman, P.J., Cooper, H.M., Coyle, M., Craig, E., et al. (2021). Overriding water table control on managed peatland greenhouse gas emissions. Nature *593*, 548–552.

19. Swindles, G.T., Morris, P.J., Mullan, D.J., Payne, R.J., Roland, T.P., Amesbury, M.J., Lamentowicz, M., Turner, T.E., Gallego-Sala, A., Sim, T., et al. (2019). Widespread drying of European peatlands in recent centuries. Nat. Geosci. *12*, 922–928.

20. Huang, Y., Ciais, P., Luo, Y., Zhu, D., Wang, Y., Qiu, C., Goll, D.S., Guenet, B., Makowski, D., De Graaf, I., et al. (2021). Tradeoff of $CO_2$ and CH4 emissions from global peatlands under water-table drawdown. Nat. Clim. Change *11*, 618–622.

21. Qiu, C., Zhu, D., Ciais, P., Guenet, B., Krinner, G., Peng, S., Aurela, M., Bernhofer, C., Brümmer, C., Bret-Harte, S., et al. (2018). ORCHIDEE-PEAT (revision 4596), a model for northern peatland $CO_2$, water, and energy fluxes on daily to annual scales. Geosci. Model Dev. *11*, 497–519.

22. Qiu, C., Zhu, D., Ciais, P., Guenet, B., Peng, S., Krinner, G., Tootchi, A., Ducharne, A., and Hastie, A. (2019). Modelling northern peatland area and carbon dynamics since the Holocene with the ORCHIDEE-PEAT land surface model (SVN r5488). Geosci. Model Dev. *12*, 2961–2982.

23. Kleinen, T., Brovkin, V., and Schuldt, R.J. (2012). A dynamic model of wetland extent and peat accumulation: results for the Holocene. Biogeosciences *9*, 235–248.

24. Wania, R., Ross, I., and Prentice, I.C. (2009). Integrating peatlands and permafrost into a dynamic global vegetation model: 1. Evaluation and sensitivity of physical land surface processes. Glob. Biogeochem. Cycles *23*, 1–19.

25. Wania, R., Ross, I., and Prentice, I.C. (2009). Integrating peatlands and permafrost into a dynamic global vegetation model: 2. Evaluation and sensitivity of vegetation and carbon cycle processes. Glob. Biogeochem. Cycles *23*, 1–15.

26. Müller, J., and Joos, F. (2020). Global peatland area and carbon dynamics from the Last Glacial Maximum to the present – a process-based model investigation. Biogeosciences *17*, 5285–5308.

27. Stocker, B.D., Spahni, R., and Joos, F. (2014). DYPTOP: a cost-efficient TOPMODEL implementation to simulate sub-grid spatio-temporal dynamics of global wetlands and peatlands. Geosci. Model Dev. *7*, 3089–3110.

28. Smith, B., Warlind, D., Arneth, A., Hickler, T., Leadley, P., Siltberg, J., and Zaehle, S. (2014). Implications of incorporating N cycling and N limitations on primary production in an individual-based dynamic vegetation model. Biogeosciences *11*, 2027–2054.

29. McGuire, A.D., Christensen, T.R., Hayes, D., Heroult, A., Euskirchen, E., Kimball, J.S., Koven, C., Lafleur, P., Miller, P.A., Oechel, W., et al. (2012). An assessment of the carbon balance of Arctic tundra: comparisons among observations, process models, and atmospheric inversions. Biogeosciences *9*, 3185–3204.

30. Chaudhary, N., Miller, P.A., and Smith, B. (2017). Modelling Holocene peatland dynamics with an individual-based dynamic vegetation model. Biogeosciences *14*, 2571–2596.

31. Xu, J., Morris, P.J., Liu, J., and Holden, J. (2018). PEATMAP: refining estimates of global peatland distribution based on a meta-analysis. Catena *160*, 134–140.

32. Frieler, K., Lange, S., Piontek, F., Reyer, C.P.O., Schewe, J., Warszawski, L., Zhao, F., Chini, L., Denvil, S., and Emanuel, K. (2017). Assessing the impacts of 1.5 C global warming–simulation protocol of the inter-sectoral impact model intercomparison project (ISIMIP2b). Geosci. Model Dev. *10*, 4321–4345.

33. Brown, J., Ferrians, O., Heginbottom, J.A., and Melnikov, E.S. (2002). Circum-Arctic Map of Permafrost and Ground-Ice Conditions, Version 2 (NSIDC: National Snow and Ice Data Center).

34. Frolking, S., Talbot, J., Jones, M.C., Treat, C.C., Kauffman, J.B., Tuittila, E.-S., and Roulet, N.T. (2011). Peatlands in the Earth's 21st century climate system. Environ. Rev. *19*, 371–396.

35. Dorrepaal, E., Toet, S., Van Logtestijn, R.S.P., Swart, E., Van De Weg, M.J., Callaghan, T.V., and Aerts, R. (2009). Carbon respiration from subsurface peat accelerated by climate warming in the subarctic. Nature *460*, 616–619.

36. Fenner, N., and Freeman, C. (2011). Drought-induced carbon loss in peatlands. Nat. Geosci. *4*, 895–900.

37. Ito, A., Reyer, C.P.O., Gädeke, A., Ciais, P., Chang, J., Chen, M., François, L., Forrest, M., Hickler, T., Ostberg, S., et al. (2020). Pronounced and unavoidable impacts of low-end global warming on northern high-latitude land ecosystems. Environ. Res. Lett. *15*, 044006.

38. Treat, C.C., Bloom, A.A., and Marushchak, M.E. (2018). Nongrowing season methane emissions–a significant component of annual emissions across northern ecosystems. Glob. Change Biol *24*, 3331–3343.

39. Peltola, O., Vesala, T., Gao, Y., Räty, O., Alekseychik, P., Aurela, M., Chojnicki, B., Desai, A.R., Dolman, A.J., and Euskirchen, E.S. (2019). Monthly gridded data product of northern wetland methane emissions based on upscaling eddy covariance observations. Earth Syst. Sci. Data *11*, 1263–1289.

40. Cain, M., Lynch, J., Allen, M.R., Fuglestvedt, J.S., Frame, D.J., and Macey, A.H. (2019). Improved calculation of warming-equivalent emissions for short-lived climate pollutants. NPJ Clim. Atmos. Sci. *2*, 1–7.

41. McGuire, A.D., Lawrence, D.M., Koven, C., Clein, J.S., Burke, E., Chen, G., Jafarov, E., MacDougall, A.H., Marchenko, S., Nicolsky, D., et al. (2018). Dependence of the evolution of carbon dynamics in the northern permafrost region on the trajectory of climate change. Proc. Natl. Acad. Sci. U S A. *115*, 3882–3887.

42. Turetsky, M.R., Abbott, B.W., Jones, M.C., Anthony, K.W., Olefeldt, D., Schuur, E.A.G., Grosse, G., Kuhry, P., Hugelius, G., Koven, C., et al. (2020). Carbon release through abrupt permafrost thaw. Nat. Geosci. *13*, 138–143.

43. Sannel, A.B.K., and Kuhry, P. (2011). Warming-induced destabilization of peat plateau/thermokarst lake complexes. J. Geophys. Res. Biogeosciences *116*, G03035.

44. Martin, L.C.P., Nitzbon, J., Aas, K.S., Etzelmüller, B., Kristiansen, H., and Westermann, S. (2019). Stability conditions of peat plateaus and palsas in northern Norway. J. Geophys. Res. Earth Surf. *124*, 705–719.

45. Aas, K.S., Martin, L., Nitzbon, J., Langer, M., Boike, J., Lee, H., Berntsen, T.K., and Westermann, S. (2019). Thaw processes in ice-rich permafrost landscapes represented with laterally coupled tiles in a land surface model. Cryosphere *13*, 591–609.

46. Shi, X., Thornton, P.E., Ricciuto, D.M., Hanson, P.J., Mao, J., Sebestyen, S.D., Griffiths, N.A., and Bisht, G. (2015). Representing northern peatland microtopography and hydrology within the Community Land Model. Biogeosciences *12*, 6463–6477.

47. Wu, Y., Verseghy, D.L., and Melton, J.R. (2016). Integrating peatlands into the coupled Canadian land surface scheme (CLASS) v3.6 and the Canadian terrestrial ecosystem model (CTEM) v2.0. Geosci. Model Dev. *9*, 2639–2663.

48. Bechtold, M., De Lannoy, G.J.M., Koster, R.D., Reichle, R.H., Mahanama, S.P., Bleuten, W., Bourgault, M.A., Brümmer, C., Burdun, I., Desai, A.R., et al. (2019). PEAT-CLSM: a specific treatment of peatland hydrology in the NASA catchment land surface model. J. Adv. Model. Earth Syst. *11*, 2130–2162.

49. Bechtold, M., De Lannoy, G.J.M., Reichle, R.H., Roose, D., Balliston, N., Burdun, I., Devito, K., Kurbatova, J., Strack, M., and Zarov, E.A. (2020). Improved groundwater table and L-band brightness temperature estimates for Northern Hemisphere peatlands using new model physics and SMOS observations in a global data assimilation framework. Remote Sens. Environ. *246*, 111805.

50. Song, J., Wan, S., Piao, S., Knapp, A.K., Classen, A.T., Vicca, S., Ciais, P., Hovenden, M.J., Leuzinger, S., Beier, C., et al. (2019). A meta-analysis of 1,119 manipulative experiments on terrestrial carbon-cycling responses to global change. Nat. Ecol. Evol. *3*, 1309–1320.

51. Bouskill, N.J., Riley, W.J., Zhu, Q., Mekonnen, Z.A., and Grant, R.F. (2020). Alaskan carbon-climate feedbacks will be weaker than inferred from short-term experiments. Nat. Commun. *11*, 1–12.

52. Andrews, T., Gregory, J.M., Webb, M.J., and Taylor, K.E. (2012). Forcing, feedbacks and climate sensitivity in CMIP5 coupled atmosphere-ocean climate models. Geophys. Res. Lett. *39*, 1–7.

53. Sherwood, S.C., Webb, M.J., Annan, J.D., Armour, K.C., Forster, P.M., Hargreaves, J.C., Hegerl, G., Klein, S.A., Marvel, K.D., Rohling, E.J., et al. (2020). An assessment of earth's climate sensitivity using multiple lines of evidence. Rev. Geophys. *58*, e2019RG000678.

54. Qiu, C., Ciais, P., Zhu, D., Guenet, B., Peng, S., Petrescu, A.M.R., Lauerwald, R., Makowski, D., Gallego-Sala, A.V., Charman, D.J., et al. (2021). Large historical carbon emissions from cultivated northern peatlands. Sci. Adv. *7*, eabf1332.

55. Gumbricht, T., Roman-Cuesta, R.M., Verchot, L., Herold, M., Wittmann, F., Householder, E., Herold, N., and Murdiyarso, D. (2017). An expert system model for mapping tropical wetlands and peatlands reveals South America as the largest contributor. Glob. Change Biol *23*, 3581–3599.

56. Frolking, S., Roulet, N., and Lawrence, D. (2009). Issues related to incorporating northern peatlands into global climate models. Carbon Cycl. North. Peatlands, 19–35.

57. Frost, G.V., and Epstein, H.E. (2014). Tall shrub and tree expansion in Siberian tundra ecotones since the 1960s. Glob. Change Biol *20*, 1264–1277.

58. Malhotra, A., Brice, D., Childs, J., Graham, J., Hobbie, E., Vander Stel, H., Feron, S., Hanson, P., and Iversen, C. (2020). Peatland warming strongly increases fine-root growth. Proc. Natl. Acad. Sci. U S A *117*, 17627–17634.

59. Hoosbeek, M.R., Van Breemen, N., Berendse, F., Grosvernier, P., Vasander, H., and Wallén, B. (2001). Limited effect of increased atmospheric $CO_2$ concentration on ombrotrophic bog vegetation. New Phytol. *150*, 459–463.

60. Wang, J., Zhu, T., Ni, H., Zhong, H., Fu, X., and Wang, J. (2013). Effects of elevated $CO_2$ and nitrogen deposition on ecosystem carbon fluxes on the Sanjiang plain wetland in Northeast China. PLoS ONE *8*, e66563.

61. Price, J.S. (2003). Role and character of seasonal peat soil deformation on the hydrology of undisturbed and cutover peatlands. Water Resour. Res. *39*, 1241.

62. Page, S.E., and Baird, A.J. (2016). Peatlands and global change: response and resilience. Annu. Rev. Environ. Resour. *41*, 35–57.

63. Treat, C.C., Wollheim, W.M., Varner, R.K., Grandy, A.S., Talbot, J., and Frolking, S. (2014). Temperature and peat type control $CO_2$ and CH4 production in Alaskan permafrost peats. Glob. Change Biol. *20*, 2674–2686.

64. Sitch, S., Smith, B., Prentice, I.C., Arneth, A., Bondeau, A., Cramer, W., Kaplan, J.O., Levis, S., Lucht, W., Sykes, M.T., et al. (2003). Evaluation of ecosystem dynamics, plant geography and terrestrial carbon cycling in the LPJ dynamic global vegetation model. Glob. Change Biol. *9*, 161–185.

65. Meinshausen, M., Smith, S.J., Calvin, K., Daniel, J.S., Kainuma, M.L.T., Lamarque, J.-F., Matsumoto, K., Montzka, S.A., Raper, S.C., Riahi, K., et al. (2011). The RCP greenhouse gas concentrations and their extensions from 1765 to 2300. Clim. Change *109*, 213–241.

66. Jones, M.C., and Yu, Z. (2010). Rapid deglacial and early Holocene expansion of peatlands in Alaska. Proc. Natl. Acad. Sci. U S A *107*, 7347–7352.

67. Morris, P.J., Swindles, G.T., Valdes, P.J., Ivanovic, R.F., Gregoire, L.J., Smith, M.W., Tarasov, L., Haywood, A.M., and Bacon, K.L. (2018). Global peatland initiation driven by regionally asynchronous warming. Proc. Natl. Acad. Sci. U S A *115*, 4851–4856.

68. MacDonald, G.M., Beilman, D.W., Kremenetski, K.V., Sheng, Y., Smith, L.C., and Velichko, A.A. (2006). Rapid early development of circumarctic peatlands and atmospheric CH4 and $CO_2$ variations. Science *314*, 285–288.

69. Pulliainen, J., Luojus, K., Derksen, C., Mudryk, L., Lemmetyinen, J., Salminen, M., Ikonen, J., Takala, M., Cohen, J., Smolander, T., et al. (2020). Patterns and trends of Northern Hemisphere snow mass from 1980 to 2018. Nature *581*, 294–298.

70. Allen, M.R., Shine, K.P., Fuglestvedt, J.S., Millar, R.J., Cain, M., Frame, D.J., and Macey, A.H. (2018). A solution to the misrepresentations of $CO_2$-equivalent emissions of short-lived climate pollutants under ambitious mitigation. Npj Clim. Atmos. Sci. *1*, 1–8.

71. Lynch, J., Cain, M., Pierrehumbert, R., and Allen, M. (2020). Demonstrating GWP*: a means of reporting warming-equivalent emissions that captures the contrasting impacts of short- and long-lived climate pollutants. Environ. Res. Lett. *15*, 044023.

72. Knutti, R., and Rogelj, J. (2015). The legacy of our $CO_2$ emissions: a clash of scientific facts, politics and ethics. Clim. Change *133*, 361–373.

73. Fuglestvedt, J., Rogelj, J., Millar, R.J., Allen, M., Boucher, O., Cain, M., Forster, P.M., Kriegler, E., and Shindell, D. (2018). Implications of possible interpretations of'greenhouse gas balance' in the Paris Agreement. Philos. Trans. R. Soc. A. Math. Phys. Eng. Sci. *376*, 20160445.

74. Tokarska, K.B., Gillett, N.P., Weaver, A.J., Arora, V.K., and Eby, M. (2016). The climate response to five trillion tonnes of carbon. Nat. Clim. Change *6*, 851–855.

75. Gillett, N.P., Arora, V.K., Matthews, D., and Allen, M.R. (2013). Constraining the ratio of global warming to cumulative $CO_2$ emissions using CMIP5 simulations. J. Clim. *26*, 6844–6858.

76. Steinacher, M., and Joos, F. (2016). Transient Earth system responses to cumulative carbon dioxide emissions: Linearities, uncertainties, and probabilities in an observation-constrained model ensemble. Biogeosciences *13*, 1071–1103.

77. Guimberteau, M., Zhu, D., Maignan, F., Huang, Y., Yue, C., Dantec-Nédélec, S., Ottlé, C., Jornet-Puig, A., Bastos, A., Laurent, P., et al. (2018). ORCHIDEE-MICT (v8. 4.1), a land surface model for the high latitudes: model description and validation. Geosci. Model Dev. *11*, 121–163.

**One Earth, Volume *5***

## Supplemental information

# A strong mitigation scenario maintains climate neutrality of northern peatlands

**Chunjing Qiu, Philippe Ciais, Dan Zhu, Bertrand Guenet, Jinfeng Chang, Nitin Chaudhary, Thomas Kleinen, XinYu Li, Jurek Müller, Yi Xi, Wenxin Zhang, Ashley Ballantyne, Simon C. Brewer, Victor Brovkin, Dan J. Charman, Adrian Gustafson, Angela V. Gallego-Sala, Thomas Gasser, Joseph Holden, Fortunat Joos, Min Jung Kwon, Ronny Lauerwald, Paul A. Miller, Shushi Peng, Susan Page, Benjamin Smith, Benjamin D. Stocker, A. Britta K. Sannel, Elodie Salmon, Guy Schurgers, Narasinha J. Shurpali, David Wårlind, and Sebastian Westermann**

**Note S1**

The models varied in their representation of peat soil carbon decomposition/accumulation processes (Table S1). Out of the five models, three (LPJ-MPI, LPX-Bern and LPJ-GUESS) assume that the peat carbon profile consists of two parts—upper layers (acrotelm) experiencing a fluctuating water table, with the decomposition of litter and SOC depending on the position of the water table; and lower layers (catotelm) being permanently saturated. Decomposition in the acrotelm is relatively fast owing to aerobic conditions above the water table, while decomposition is slow under anaerobic conditions of the catotelm. The other two models (ORCHIDEE-PEAT and LPJ-GUESS_dynP) represent the peat profile as a multi-layered soil profile, with the respiration in each layer being controlled by soil temperature and moisture of the layer. ORCHIDEE-PEAT uses a downward transport of carbon between soil layers to simulate the accumulation of peat, with the intrinsic decomposition rate of SOC decreasing with depth.[1] In LPJ-GUESS_dynP, a new layer of peat is deposited over previously accumulated peat layers each year, and the intrinsic decomposition rate of SOC decreases over time.[2] These five models also differ in their parameterizations of peatland-specific vegetation, the inundation stress on plants, and carbon–nitrogen cycle interactions (Table S1).

The models encompass a wide spectrum of complexity in features that determine peat soil hydrological and thermal dynamics (Table S2). These range from models (LPJ-MPI, LPX-Bern, LPJ-GUESS and LPJ-GUESS_dynP) that apply a water bucket scheme to a model (ORCHIDEE-PEAT) that simulates a physically-based unsaturated soil water flow (using a one-dimensional Fokker-Planck equation [3]), from an empirical model which calculates soil temperature from the air temperature (LPJ-MPI) to a physically-based model which mechanistically simulates the radiative energy balance, soil freezing and thawing and phase change-induced heat fluxes in the soil (ORCHIDEE-PEAT), and from a simple single-layer snow scheme (LPJ-GUESS, LPX-Bern, LPJ-GUESS_dynP) to a 3-layer snow scheme of intermediate complexity (ORCHIDEE-PEAT). Some models include the thermal insulation effect of soil organic matter while the others do not (Table S2).

The models also varied in their parameterization of $CH_4$ emissions from peatlands. Pathways and availability of carbon substrate, $CH_4$ production, oxidation and transport processes differ to some extent from model to model (Table S3).

Greenhouse gas emissions from peatlands are closely linked with peatland hydrological conditions. The important hydrological variable, water-table position (WTP), is calculated differently across models.

In ORCHIDEE-PEAT, the calculation of peatland WTP is based on the total water volume in the uppermost 2 m of the soil[4]:

$$WTP = H_{tot} - \sum_{i=1}^{11}\left(\theta_{fi} \times dz_i\right) - H_{ab}, \text{ with } \theta_{fi} = \frac{\theta_i - \theta_r}{\theta_s - \theta_r} \qquad (1)$$

where $\theta_{fi}$ is the relative volumetric water content of the $i$th soil layer, $\theta_i$ is the simulated water content of the soil layer, $\theta_s$ is the saturated water content, $\theta_r$ is the residual water content (the minimum soil moisture), $H_{tot}$ is the total soil column height being fixed to 2 m, $H_{ab}$ is the height of the above-surface water reservoir (maximum 10 cm), $dz_i$ is the distance between model layers.

In LPJ-MPI, peatland WTP is calculated according to TOPMODEL[5]:

$$WTP = \overline{WTP} + \frac{1}{f}(\chi_i - \bar{\chi}), \text{ with } \overline{WTP} = z_b - \left(\frac{\bar{w} - w_{thre}}{1 - w_{thre}}\right) \times \Delta_z \qquad (2)$$

where $\overline{WTP}$ is the grid cell mean water table, $\chi_i$ is the local compound topographic index (CTI) in point $i$, $\bar{\chi}$ is the grid cell mean CTI index, $f$ is a parameter describing the exponential decline of transmissivity with depth, $z_b$ is the bottom of the soil column, $\Delta_z$ is the height of the soil column, $\overline{w}$ is the soil column average soil moisture and $w_{thre}$ is the minimum soil moisture for a water table to form.

In LPJ-GUESS and LPX-Bern, peatland WTP is calculated based on the total water volume, $V_{tot}$ (mm), and the depth, $z_{acro}$, and porosity, $\phi$, of the acrotelm with the parameters $f_{water}^{surfmin}$ and $\alpha_z$ representing the minimum fractional water content at the surface and the increase of surface water content from $f_{water}^{surfmin}$ to the maximum water content, respectively[6]:

$$WTP = \begin{cases} V_{tot} - z_{acro}\phi, & WTP > 0 \\ -\sqrt{\dfrac{3(\phi z_{acro} - V_{tot})}{2\alpha_z}}, & -100 \le WTP \le 0 \\ -\dfrac{3(\phi z_{acro} - V_{tot})}{2\left(\theta - f_{water}^{surfmin}\right)}, & WTP < -100 \end{cases} \quad (3)$$

In LPJ-GUESS_dynP, the surface of a peatland is represented by uneven heights of individual patches, water is redistributed from the higher elevated patches to low depressions through lateral flow. The WTP of individual patches is equalized to match the mean WTP of the landscape. Patches lose water if their WTP is above the mean WTP of the landscape while the lower patches receive water[2]:

$$WTP = \frac{\Sigma PWTP_i}{n} \quad (4)$$

where $PWTP_i$ is the water table position in patch $i$, $n$ is the total number of patches. In the model, the water balance of peatland is modeled using a "bucket" approach, water (the difference between precipitation, evapotranspiration, runoff, vertical drainage and lateral flow within the landscape) is added to the top of the peat column formed by individual peat layers to determine $PWTP_i$.

Note that a negative WTP value means that the water table is above the surface in ORCHIDEE-PEAT and LPJ-MPI (equation 1 and 2), while it means that the water table is below the surface in LPJ-GUESS, LPX-Bern and LPJ-GUESS_dynP (equation 3 and 4). In the main text and all figures, the water-table depth (WTD) is defined as the distance of the water table to the soil surface and the sign of WTD is consistent among models; positive WTD values mean that the water table is below the surface.

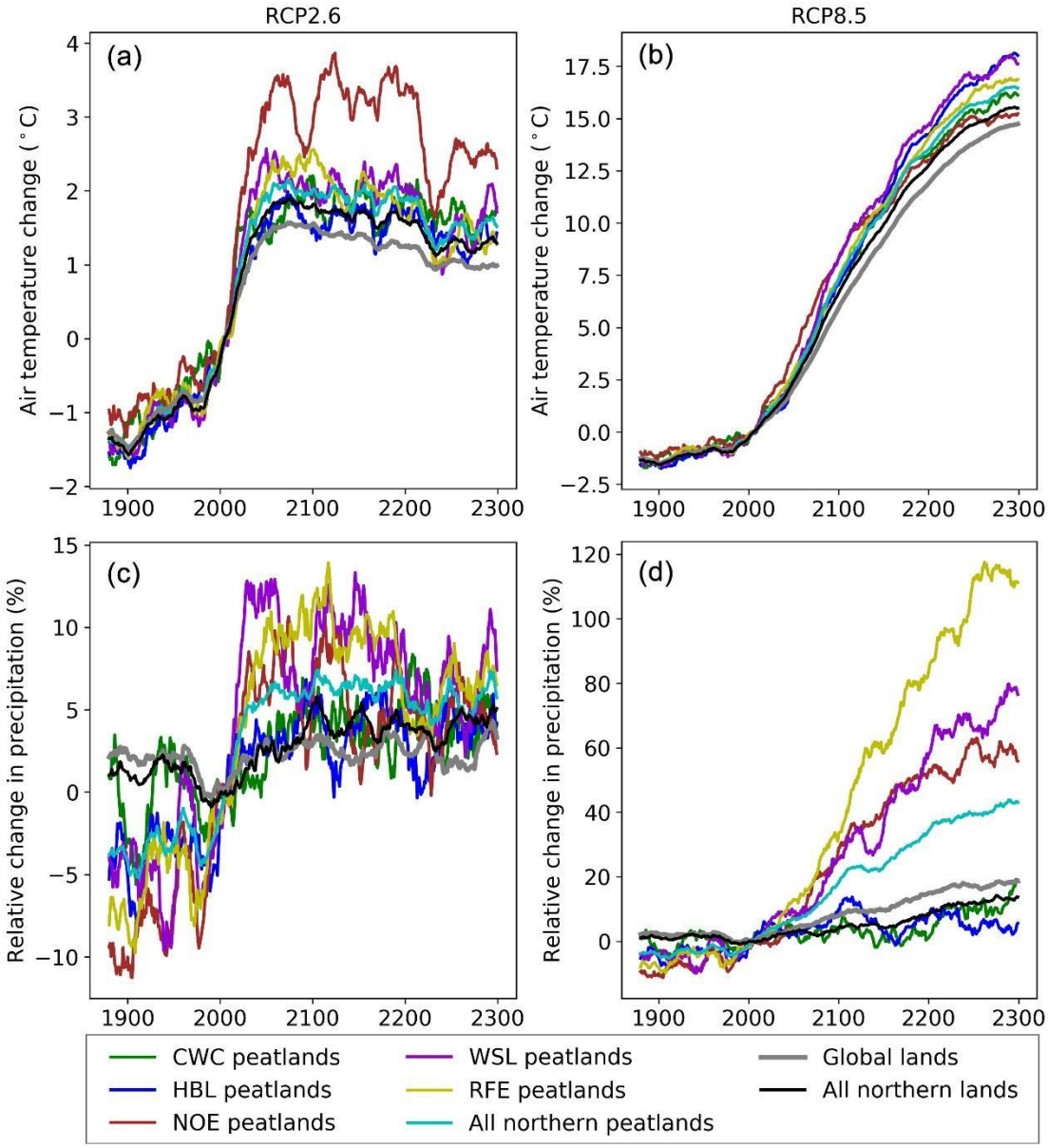


**Figure S1.** Absolute change in air temperature under RCP2.6 (a) and RCP8.5 (b), and relative change in annual precipitation under RCP2.6 (c) and RCP8.5 (d), with respect to the 1986–2005 average, projected by the IPSL-CM5A-LR general circulation model (GCM).[7] Data shown are 20-year moving averages, and moving average values were assigned to the last year of each window period. All northern lands and peatlands (> 30°N) and five sub-region peatlands have been studied. These sub-region peatlands are: Continental Western Canada (CWC), the Hudson Bay Lowlands (HBL), Northern Europe (NOE), the West Siberian Lowlands (WSL), and the Russian Far East (RFE).

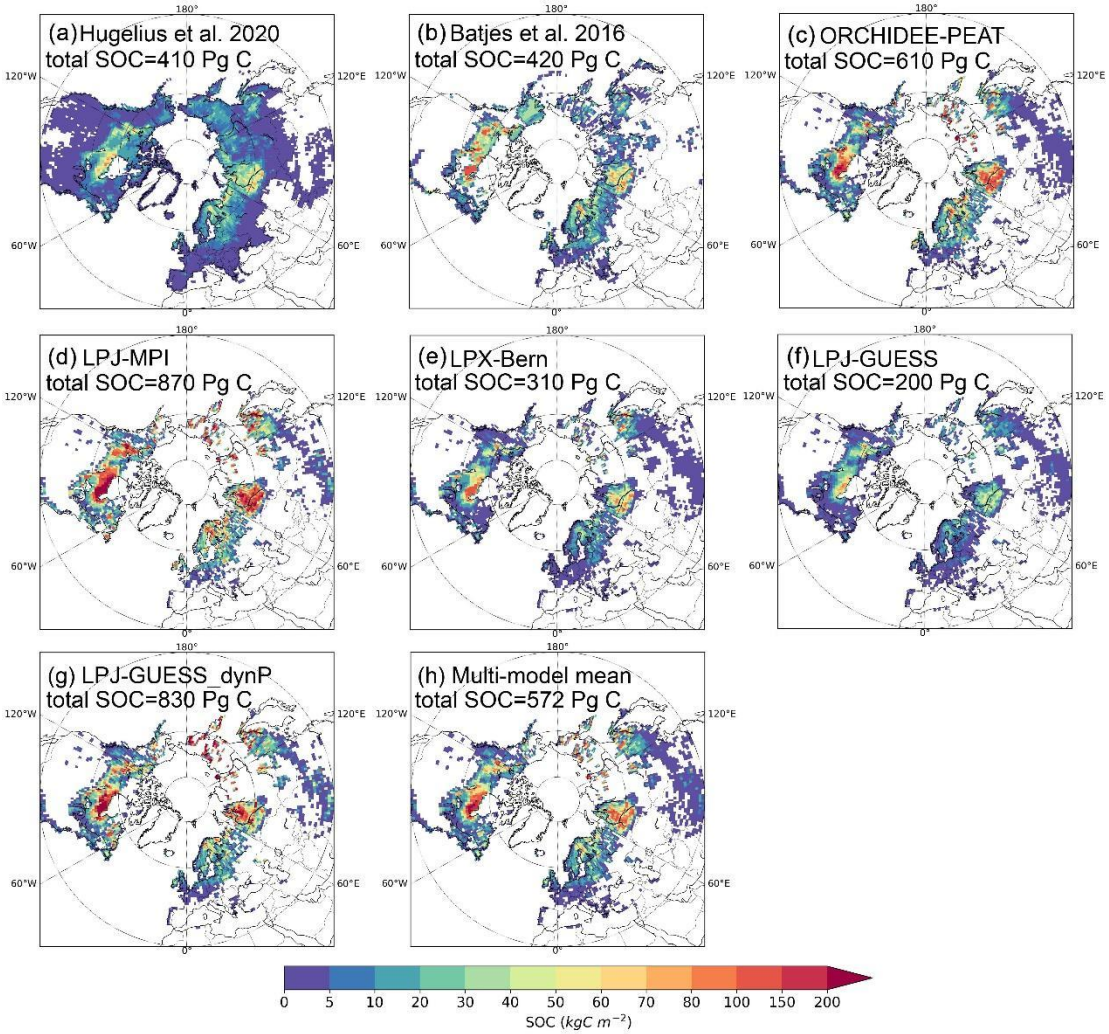


**Figure S2.** Observation-based and simulated peatland soil organic carbon density (SOC). (a) Observation-based peatland soil carbon density from Hugelius et al.[8], (b) Observation-based histosols soil carbon density from Batjes et al.[9], and simulated peatland soil carbon storage from (c) ORCHIDEE-PEAT, (d) LPJ-MPI, (e) LPX-Bern, (f) LPJ-GUESS, (g) LPJ-GUESS_dynP, and (h) multi-model ensemble mean. Note peatland area extent in (a) and (b), are different to the peatland area extent in the PEATMAP[10] dataset used in this study (c-h).

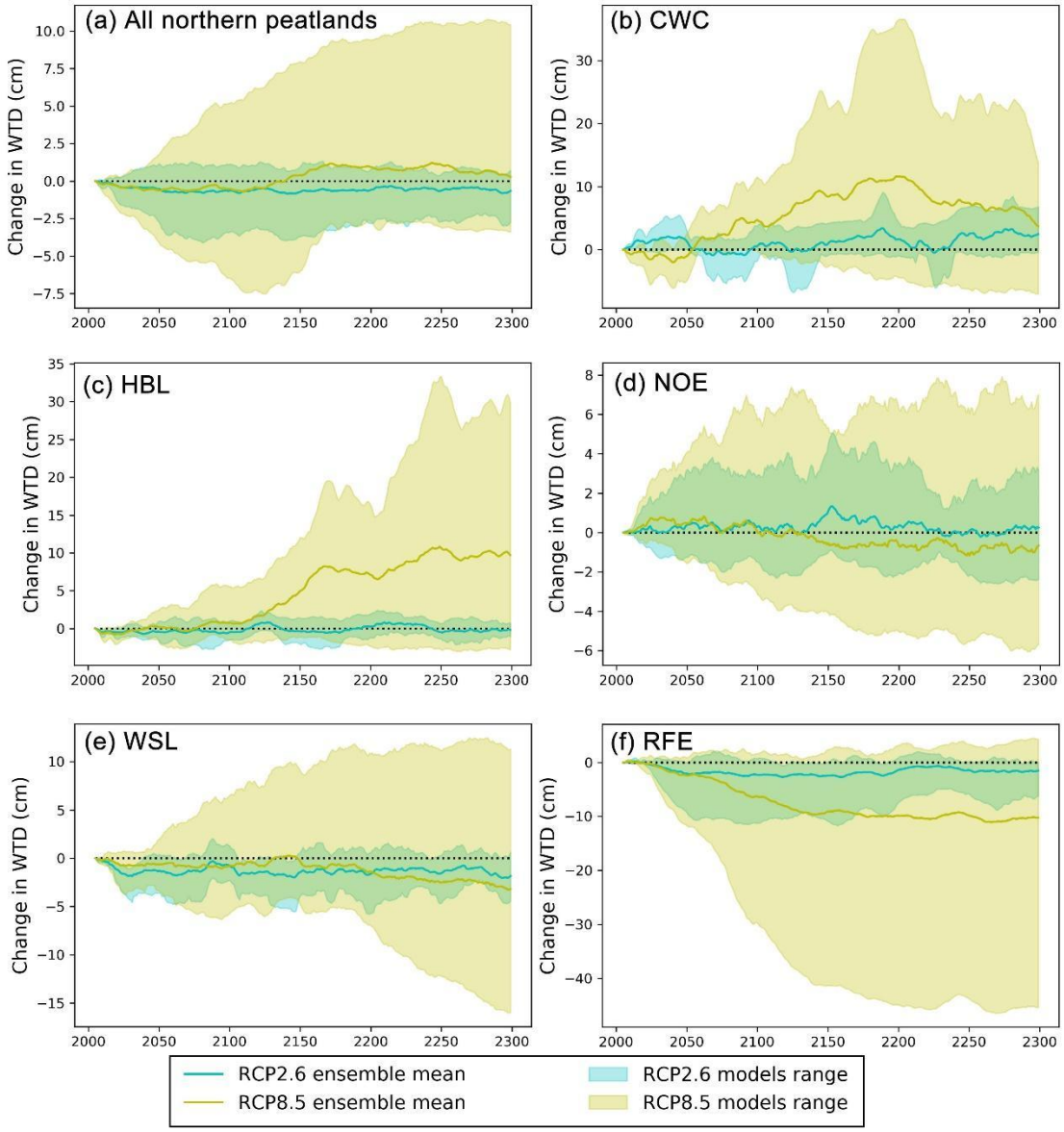


**Figure S3.** Simulated absolute change in annual mean water-table depth (WTD) defined as the distance of water table to the soil surface, with respect to the 1986–2005 average, under RCP2.6 (cyan) and RCP8.5 (yellow) for different regions. Data shown are 20-year moving averages, and moving average values were assigned to the last year of each window period. A positive value in the figure represents a deepening of the water table.

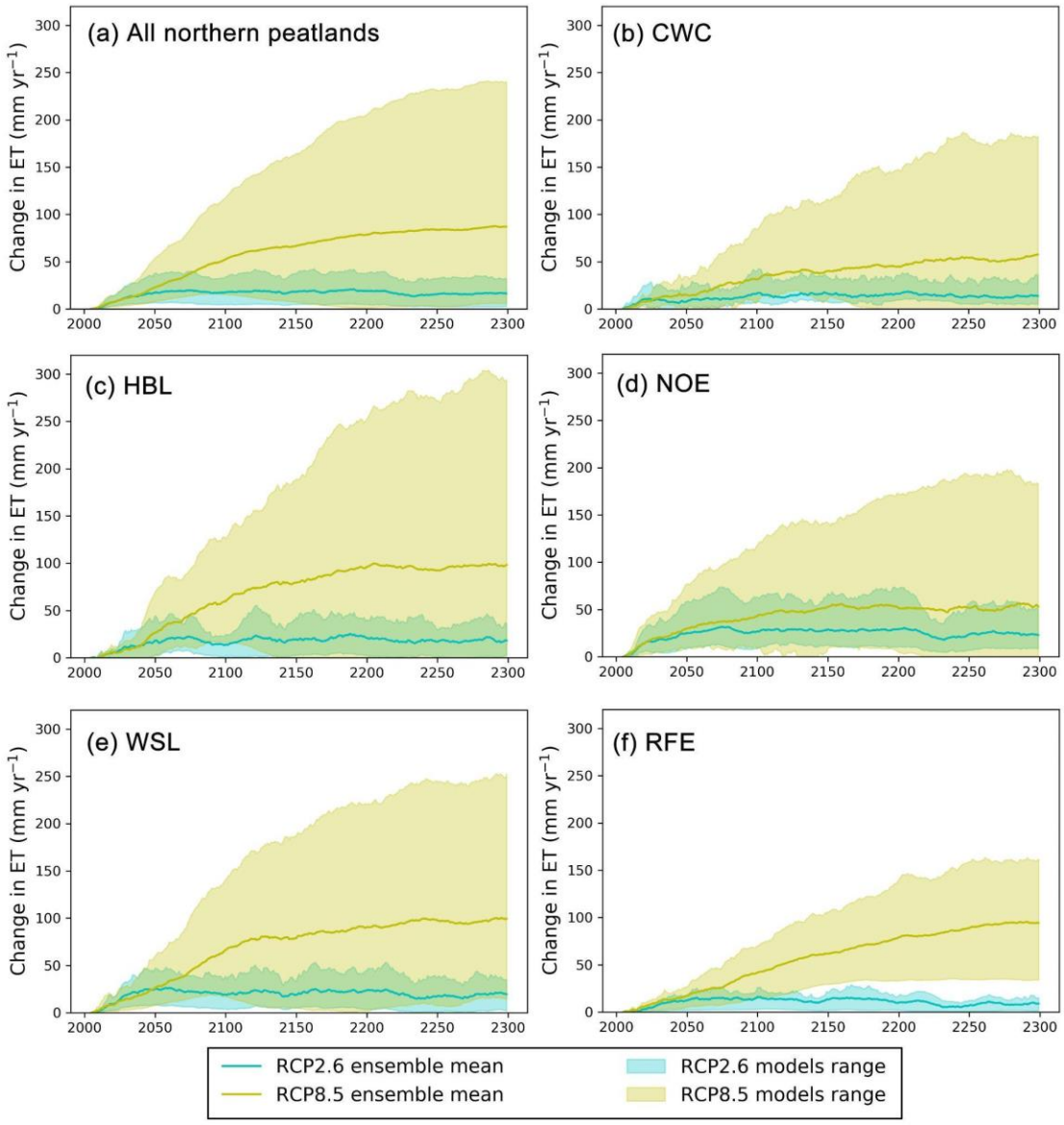


**Figure S4.** Simulated change in evapotranspiration (ET) with respect to the 1986–2005 average, under RCP2.6 (cyan) and RCP8.5 (yellow), respectively. Data shown are 20-year moving averages, and moving average values were assigned to the last year of each window period.

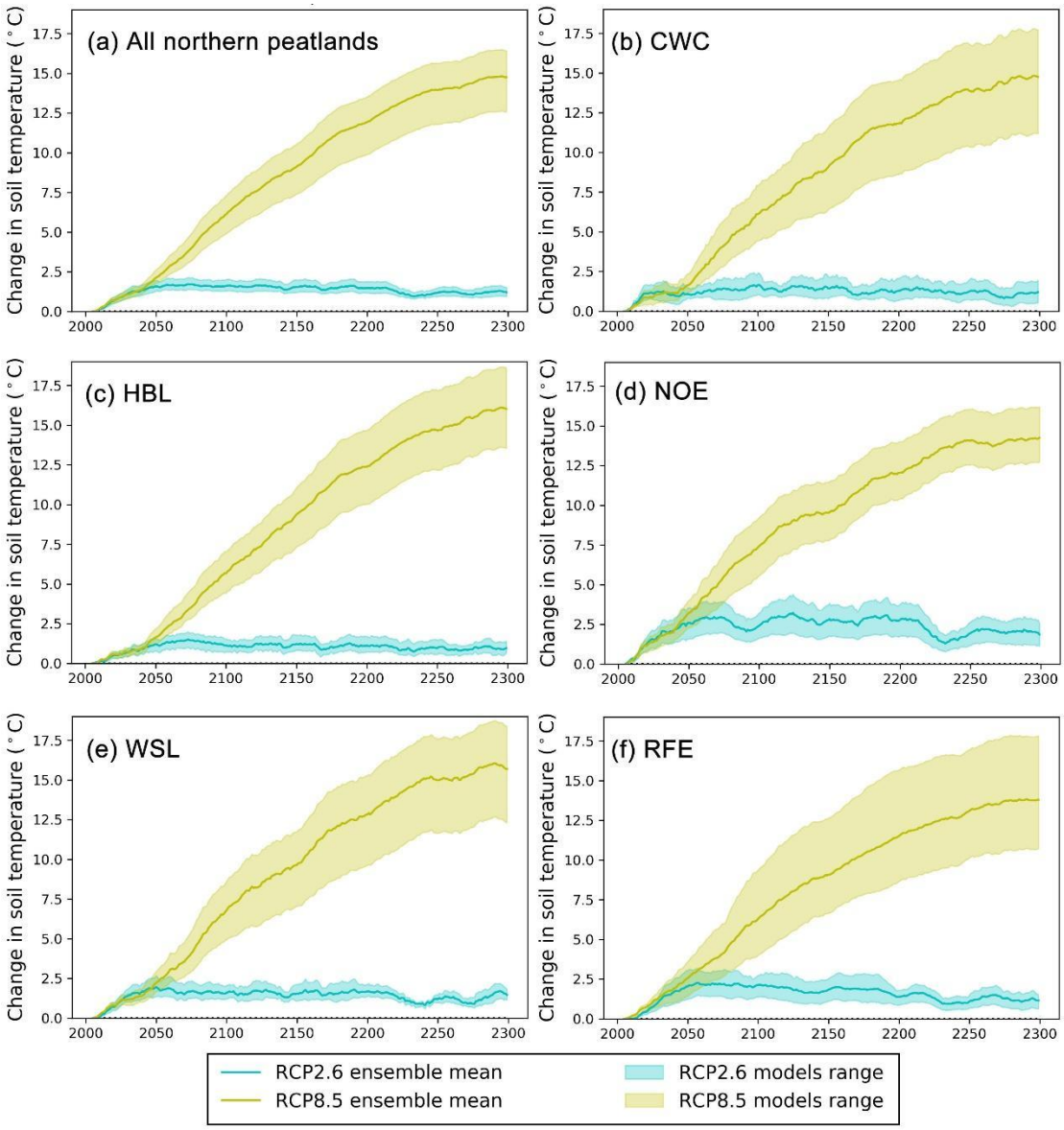


**Figure S5.** Simulated change in soil temperature (at 25 cm depth) with respect to the 1986–2005 average, under RCP2.6 (cyan) and RCP8.5 (yellow), respectively. Data shown are 20-year moving averages, and moving average values were assigned to the last year of each window period.

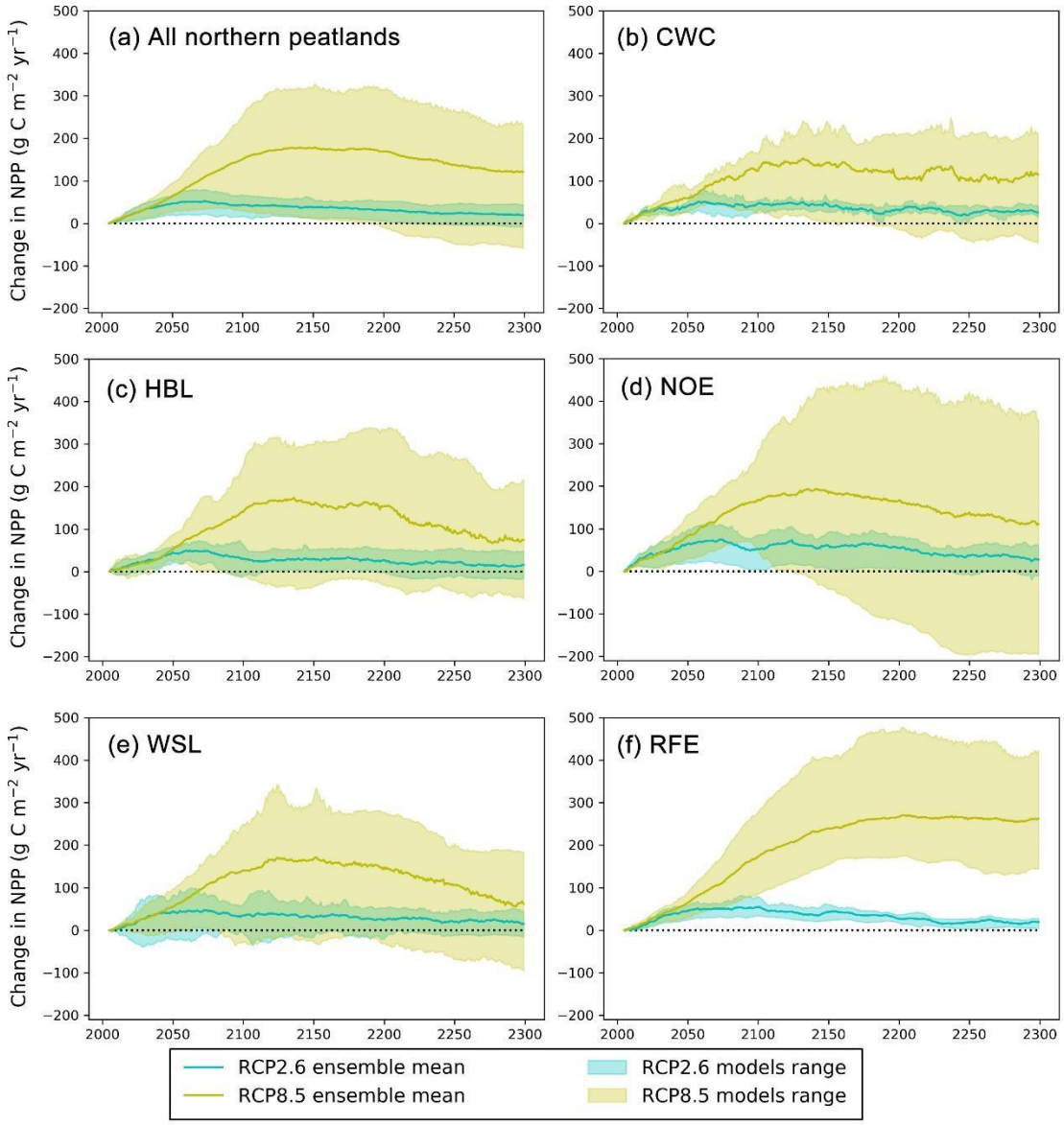


**Figure S6.** Simulated change in net primary productivity (NPP) with respect to the 1986–2005 average, under RCP2.6 (cyan) and RCP8.5 (yellow), respectively. Data shown are 20-year moving averages, and moving average values were assigned to the last year of each window period.

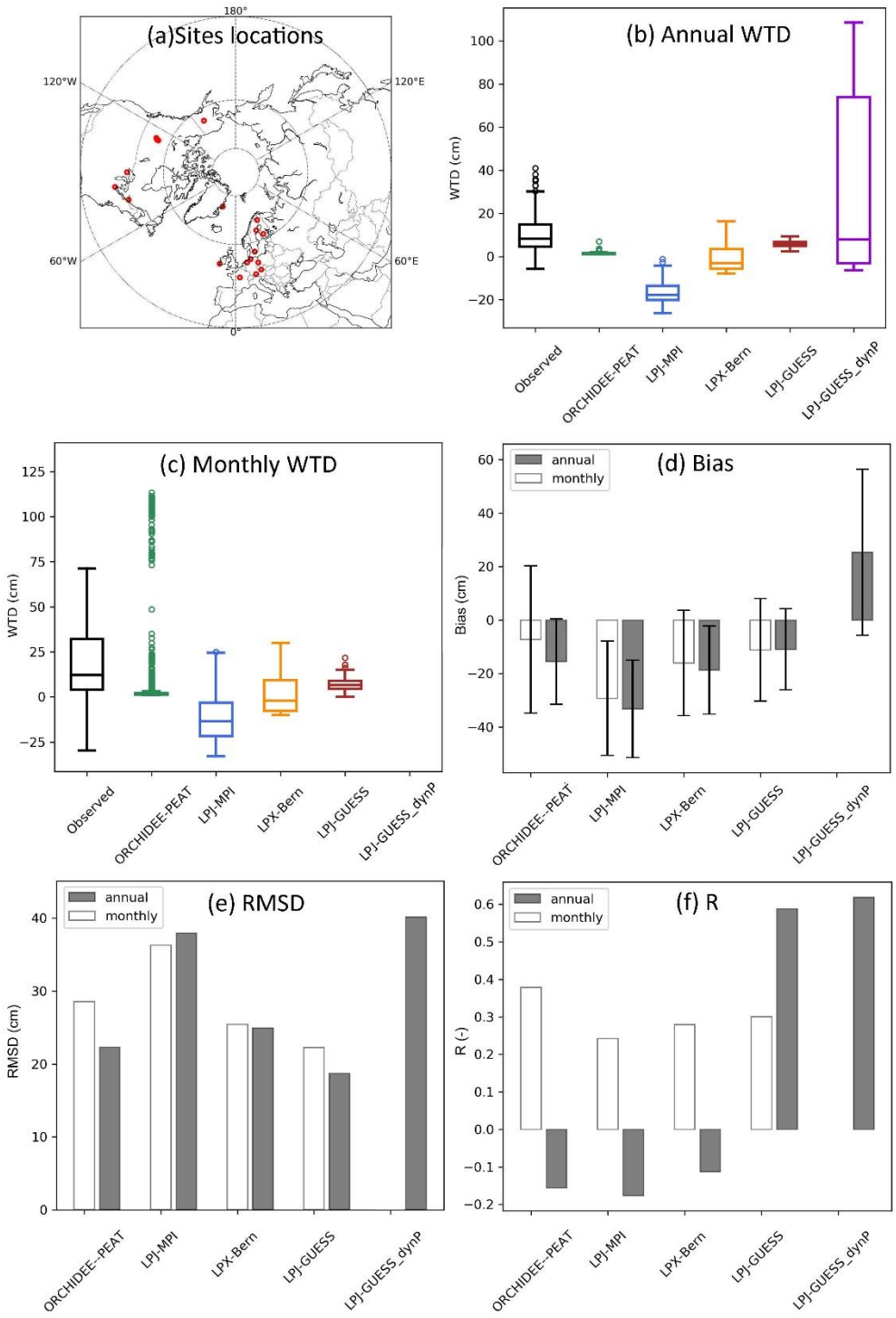


**Figure S7.** Observed and simulated peatland water-table depth (WTD) defined as the distance of water table to the soil surface, with a positive sign representing a water table below the soil surface, from 20 northern peatland sites (108 site-year measurements). (a) The distribution of peatland sites, (b) Annual mean WTD, (c) Monthly mean WTD, (d) Bias (simulated minus observed), (e) Root mean squared difference between simulated and observed WTD, (f) Pearson correlation coefficient between simulated and observed WTD (spatial correlations showing among-site variability). Site information can be found in Qiu et al.[4]. Note that peat accumulation and decomposition are simulated at an annual time step in LPJ-GUESS_dynP and thus the model is only evaluated at annual time scale.

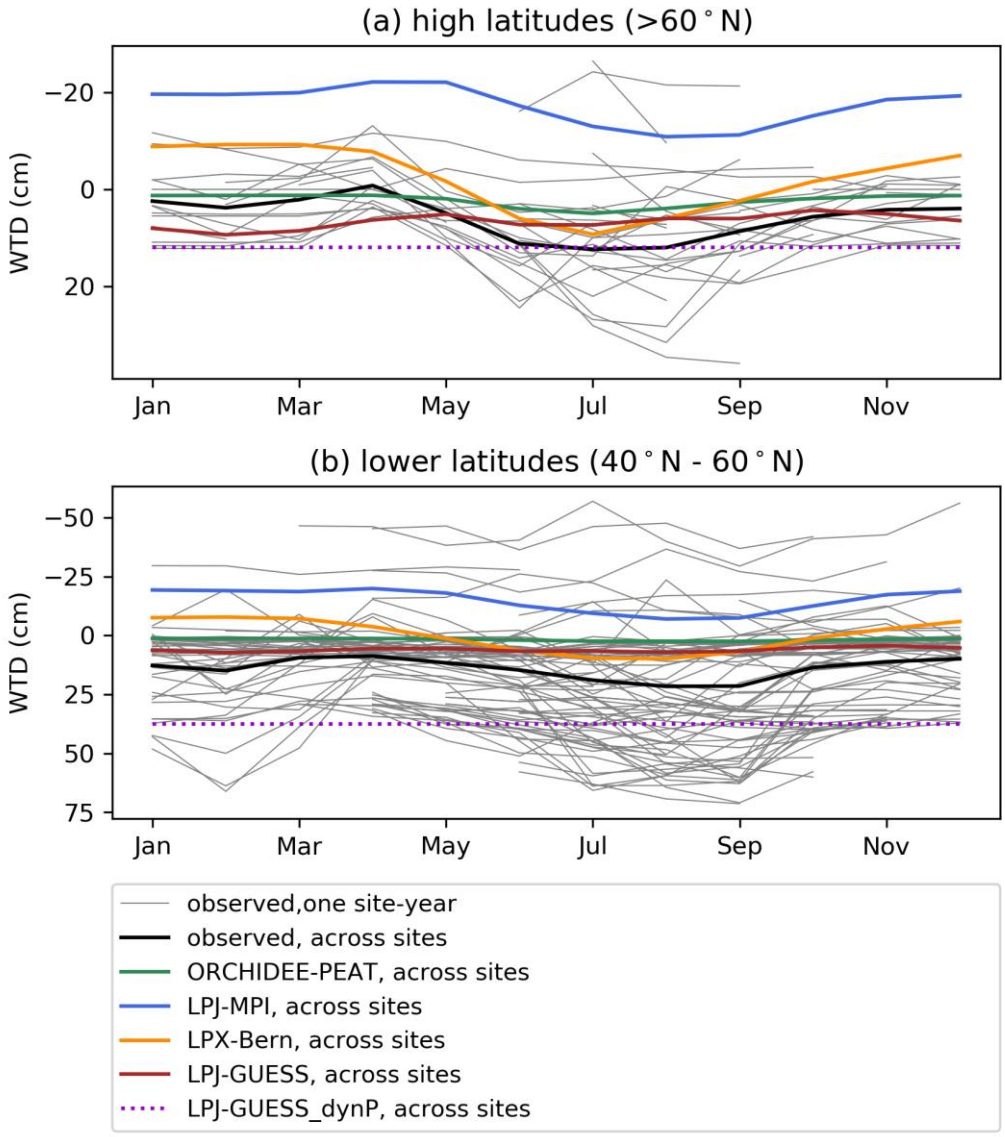


**Figure S8.** Observed and simulated water-table depth (WTD) for high latitudes sites (a), and for lower latitudes sites (b). Sites used in this figure are same to that in Figure S7. Each grey line represents one site-year of WTD measurements, while thick black and colored lines show averages of WTD measurements across all site-years. Note that peat accumulation and decomposition are simulated at an annual time step in LPJ-GUESS_dynP and thus the model is only evaluated at annual time scale.

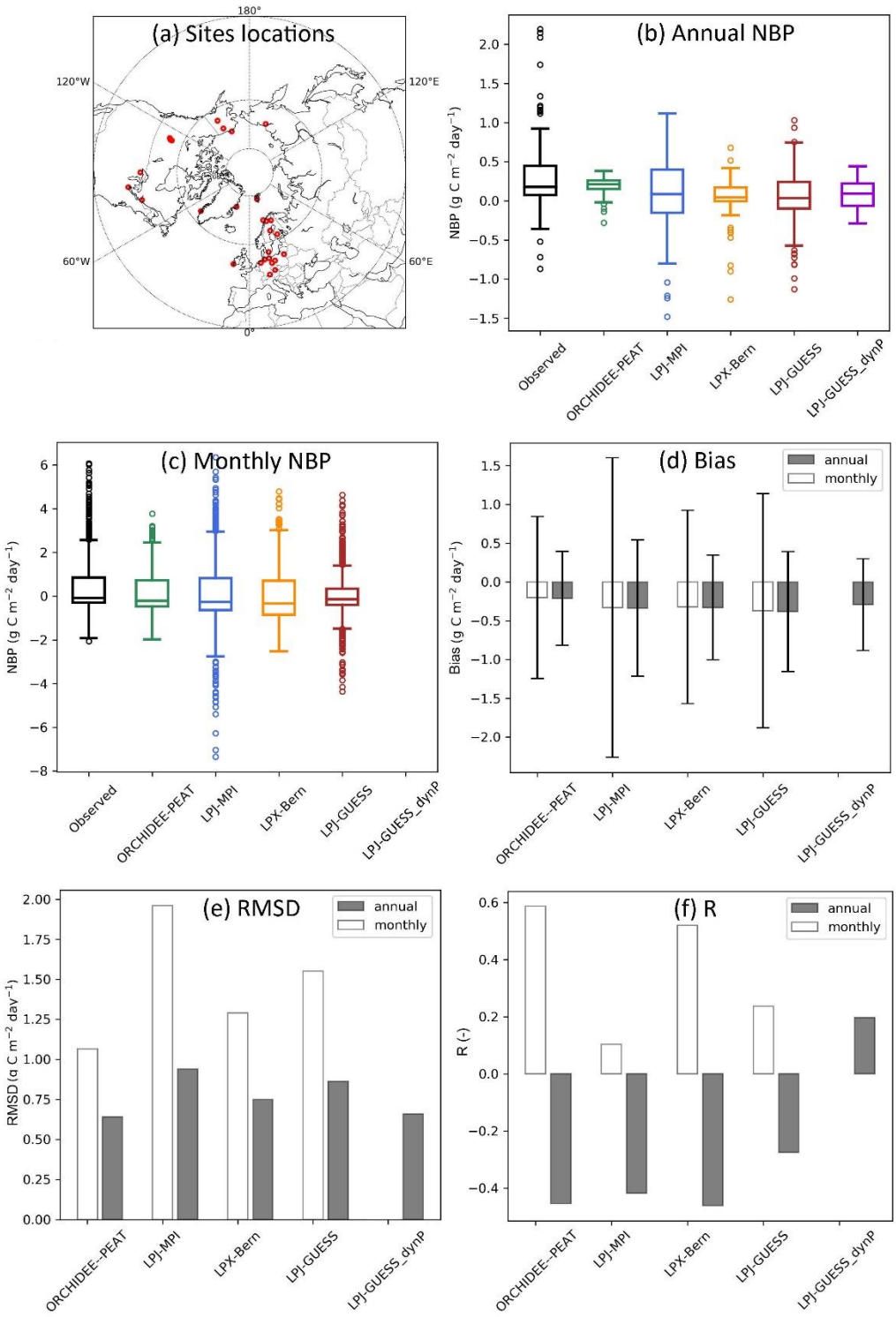


**Figure S9.** Observed and simulated peatland NBP (a positive sign represents $CO_2$ fluxes from the atmosphere to the peatland ecosystem) from 29 northern peatland sites (152 site-year flux measurements). (a) The location of the sites, (b) Annual mean NBP, (c) Monthly mean NBP, (d) Bias (simulated minus observed), (e) Root mean squared difference between simulated and observed NBP, (f) Pearson correlation coefficient between simulated and observed NBP (spatial correlations showing among-site variability). Site information can be found in Qiu et al.[4]. Note that peat accumulation and decomposition are simulated at an annual time step in LPJ-GUESS_dynP and thus the model is only evaluated at annual time scale.

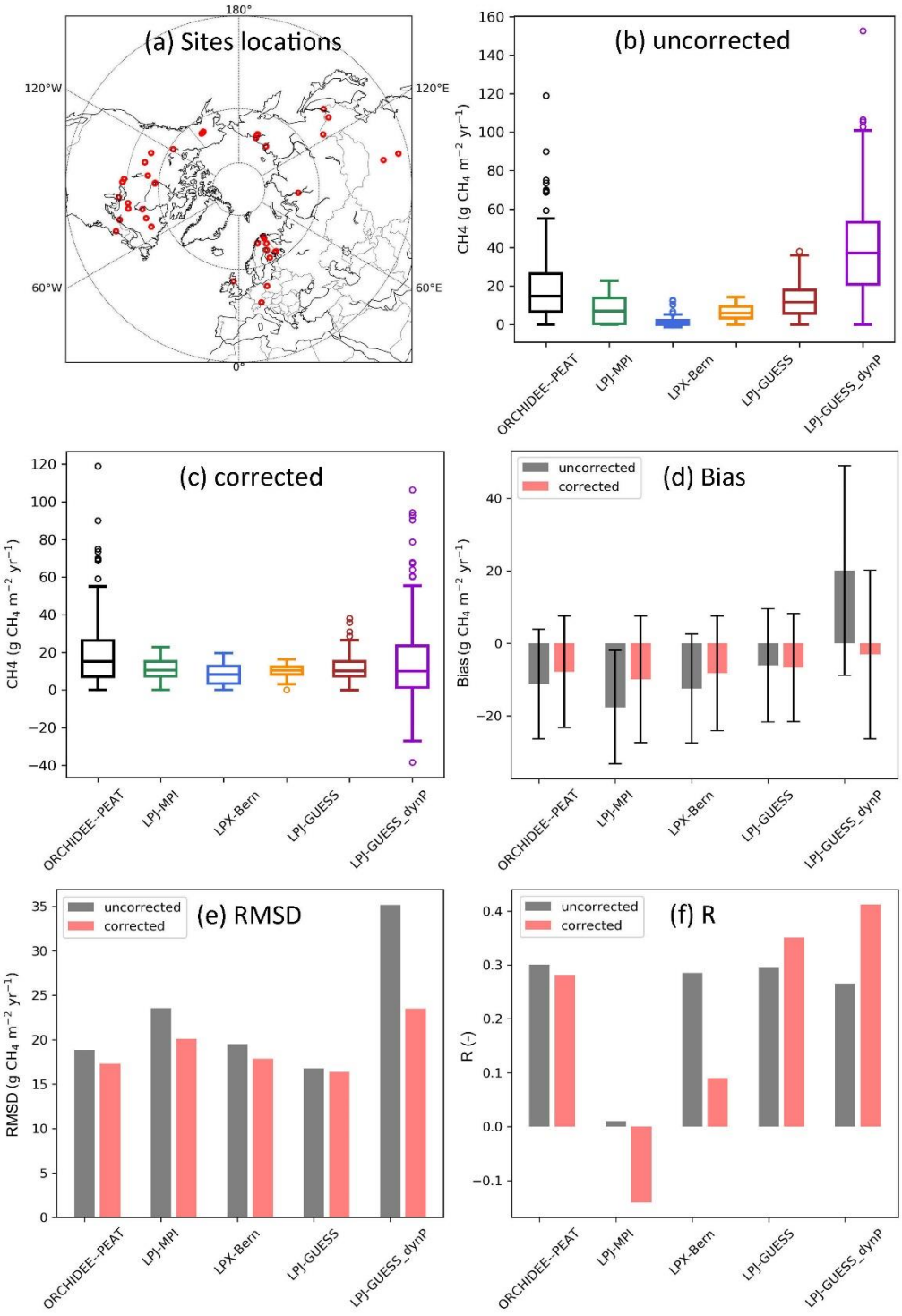


**Figure S10.** Observed and simulated peatland $CH_4$ emissions. Observations are from 81 peatland sites (419 site-year flux measurements) from Treat et al.[11]. (a) The location of the sites, (b) observed versus simulated peatland annual $CH_4$ emissions before the bias-correction, (c) observed versus simulated peatland annual $CH_4$ emissions after the bias-correction, (d) Bias (simulated minus observed), (e) Root mean squared difference between simulated and observed $CH_4$ emissions, (f) Pearson correlation coefficient between simulated and observed $CH_4$ emissions (spatial correlations showing among-site variability).

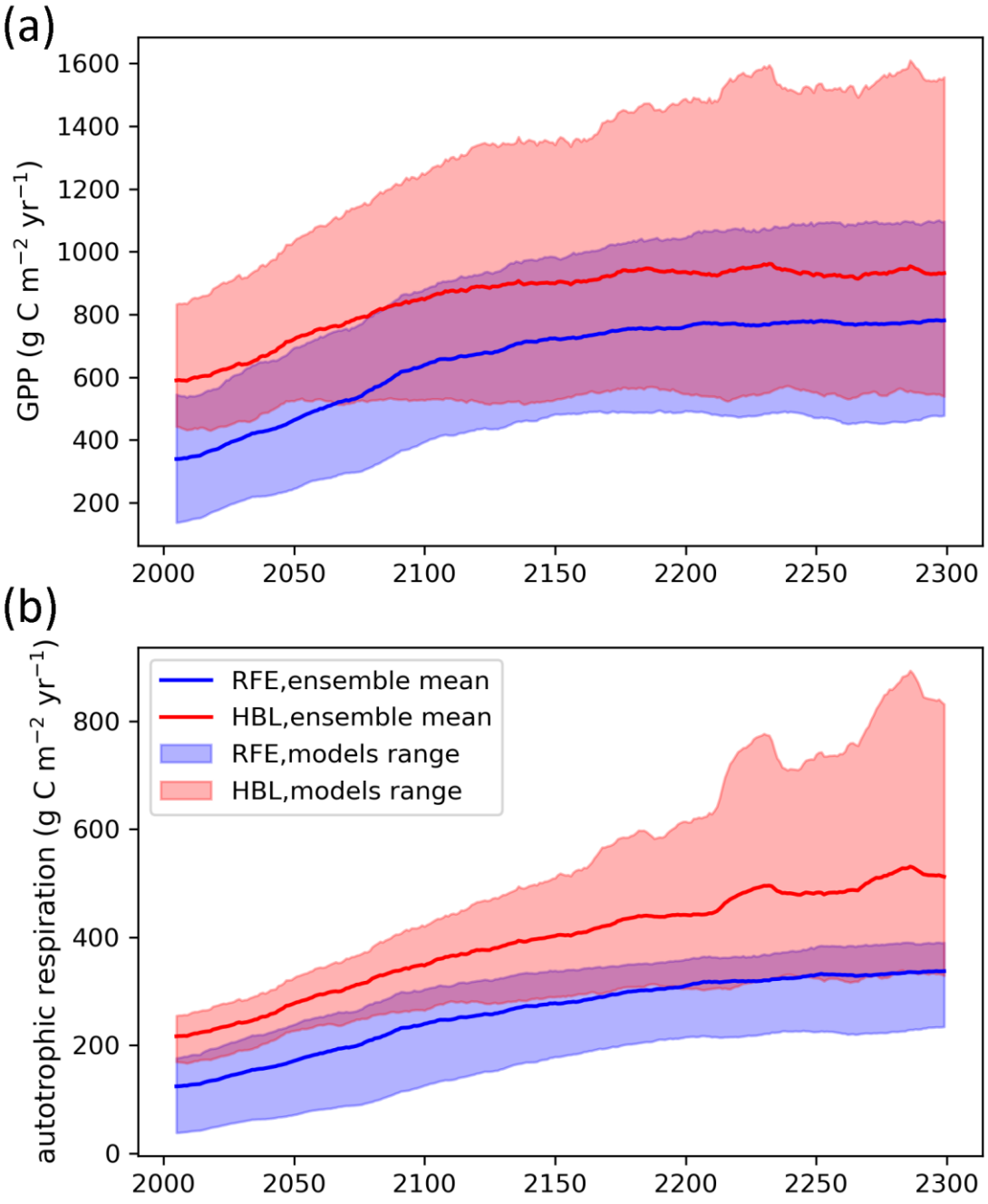


**Figure S11.** Simulated (a) gross primary productivity (GPP) and (b) plant autotrophic respiration for the Russian Far East (RFE) peatlands (blue) and Hudson Bay Lowlands (HBL) peatlands (red) under RCP8.5.

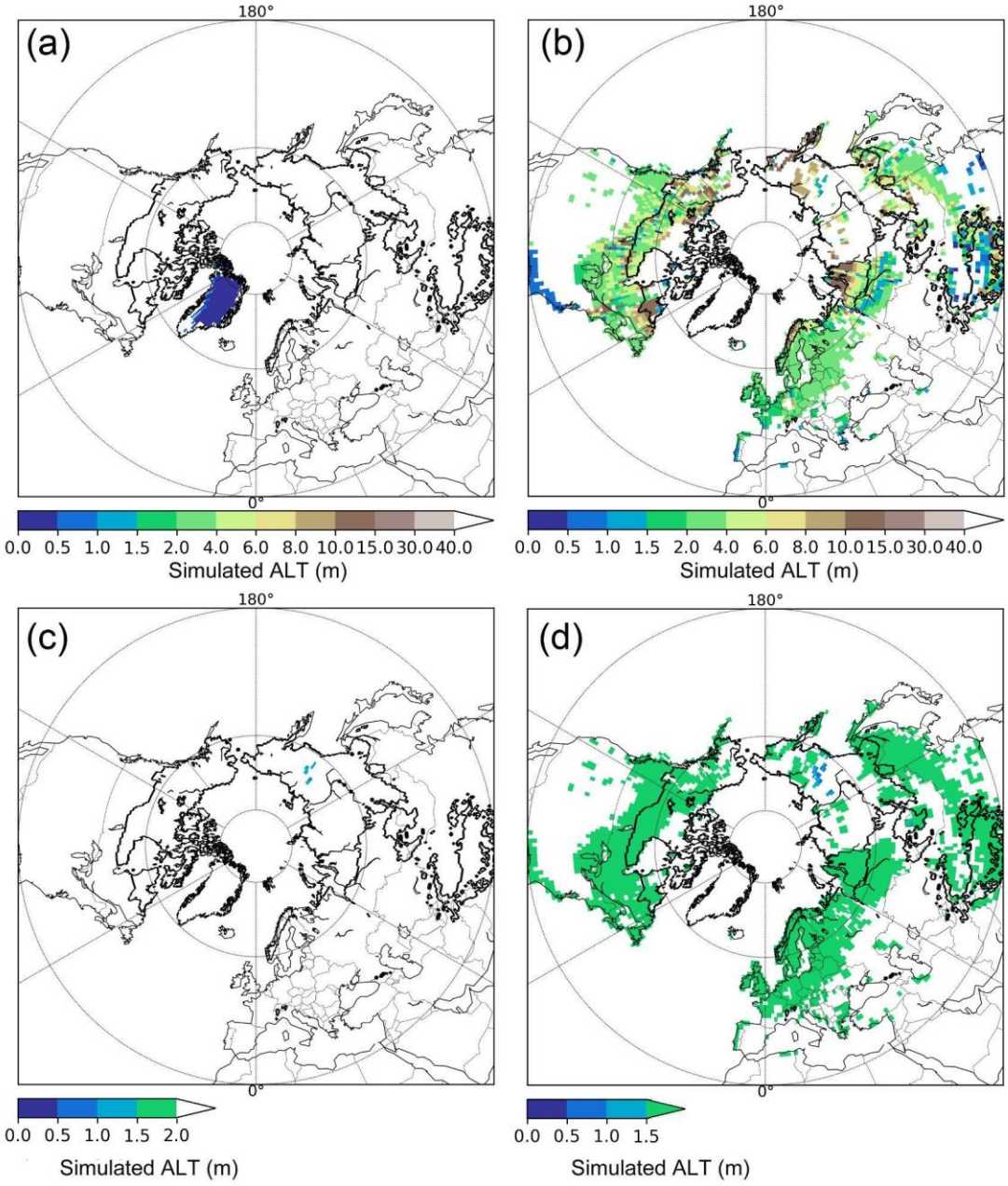


**Figure S12.** Simulated (background maps) active layer thickness (ALT) by 2300 (2280-2299 mean) under RCP8,5, from (a) ORCHIDEE-PEAT, (b) LPJ-GUESS_dynP, (c) LPX-Bern and (d) LPJ-GUESS. Note that the definition of active layer is different among models, it is defined as the maximum depth where annual average ice content>0 by LPJ-GUESS_dynP, while it is defined as the maximum thaw depth (below that soils have temperature<0 °C throughout the year) by the other three models. The definition used by LPJ-GUESS_dynP would result in a smaller ALT. The extent of continuous, discontinuous and sporadic permafrost from the IPA (International Permafrost Association) permafrost map[12] is superimposed on simulated ALT (black lines), all grid cells within this extent are regarded as "permafrost peatland" and are applied for the past and the future in the main text. The peat profile is represented by two model layers — the acrotelm layer (top 0.3 m) and the catotelm layer (1.7 m) in LPX-Bern and LPJ-GUESS, and there is no peat deeper than 2.0 m.

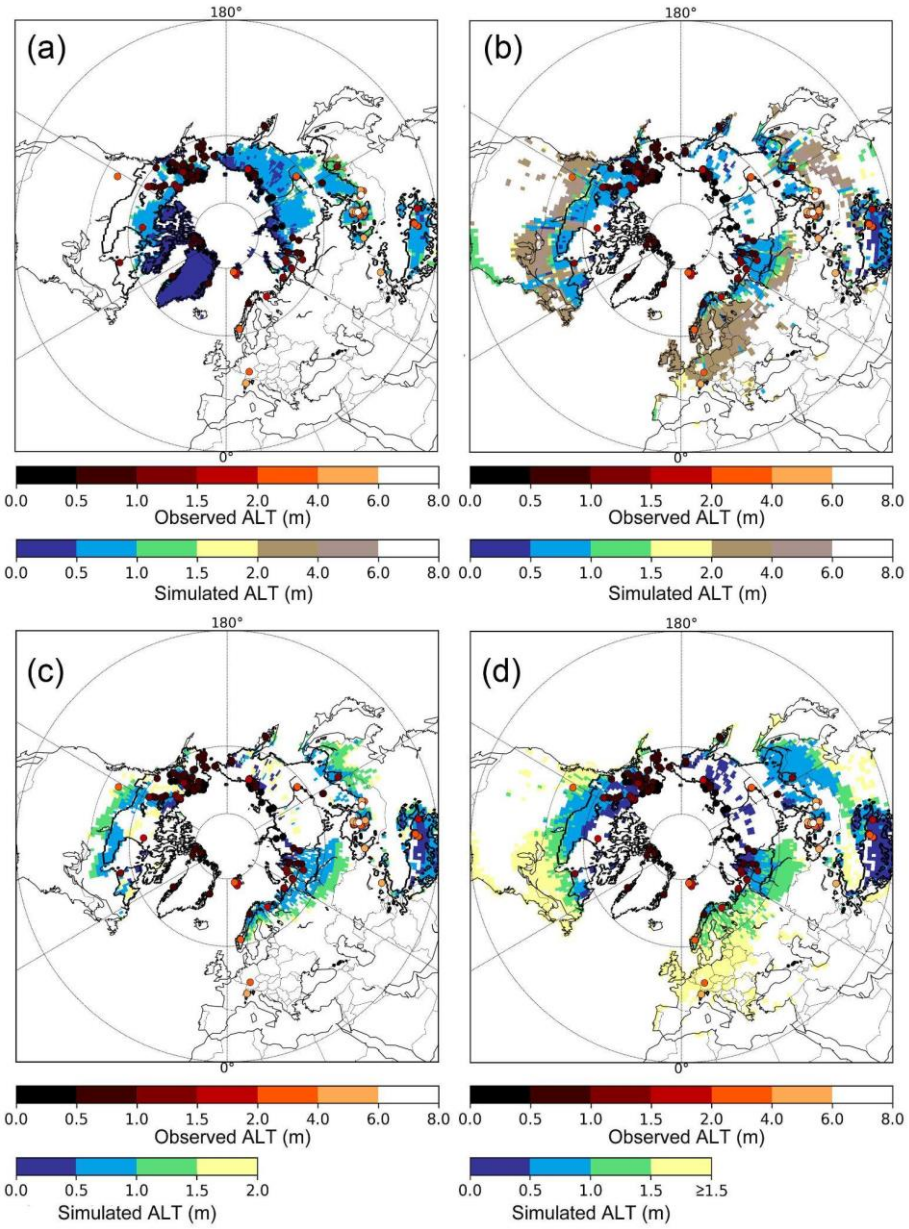


**Figure S13.** Observed (color-filled circles) and simulated (background maps) present-day (1986–2005 mean) active layer thickness (ALT) by (a) ORCHIDEE-PEAT, (b) LPJ-GUESS_dynP, (c) LPX-Bern and (d) LPJ-GUESS. Color-filled circles are in-situ observed active layer thickness from the Circumpolar Active Layer Monitoring (CALM) network. Note that the definition of active layer is different among models, it is defined as the maximum depth where annual average ice content>0 by LPJ-GUESS_dynP, while it is defined as the maximum thaw depth (below that soils have temperature<0 °C throughout the year) by the other three models. The definition used by LPJ-GUESS_dynP would result in a smaller ALT. The extent of continuous, discontinuous and sporadic permafrost from the IPA (International Permafrost Association) permafrost map[12] is superimposed on simulated ALT (black lines), all grid cells within this extent are regarded as "permafrost peatland" and are applied for the past and the future in the main text. The peat profile is represented by two model layers — the acrotelm layer (top 0.3 m) and the catotelm layer (1.7 m) in LPX-Bern and LPJ-GUESS, and there is no peat deeper than 2.0 m.

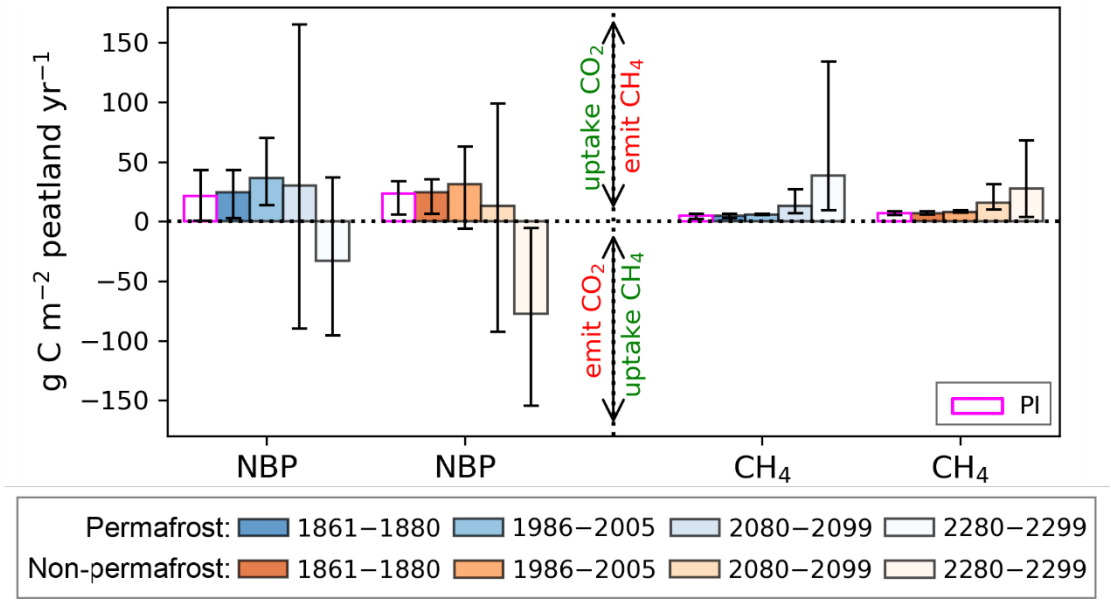


**Figure S14.** Same as Figure 5 with expected fluxes under unchanged pre-industrial (PI) conditions shown by open magenta bars.

**Table S1.** Representation of peatland vegetation, soil carbon and hydrology of participating models

| Model | Dynamic vegetation | Peatland hydrology | Inundation stress on NPP of some plant species | Soil carbon decomposition and accumulation | Carbon – Nitrogen cycle interactions |
|---|---|---|---|---|---|
| **ORCHIDEE-PEAT**[1,4] | No, only one specific, grass-like PFT representing mixed plant species in northern peatlands | **Scheme:** one-dimensional water diffusion; the Fokker-Planck equation with Van Genuchten - Mualem parameters. **Hydrological properties:** peat-specific. **Lateral water input:** yes, surface runoff from non-peatland vegetation within a grid cell containing a fraction of peatland is routed to this peatland. **Lateral water loss from peatland:** surface runoff occurs in the form of Hortonian flow. **Ponding on the surface:** yes, there is an above-surface water reservoir with a maximum height of 10 cm. **Microtopography:** not considered. | No | **Scheme:** multilayer (up to 38 m); **Accumulation:** a downward transport of carbon across soil layers; **Decomposition** controlled by soil moisture (volumetric water content) and temperature in each layer. | N cycle was not explicitly modeled, but added a down-regulation of photosynthesis as $CO_2$ increases to represent nutrient constraints |

| | | | | | |
|---|---|---|---|---|---|
| **LPJ-GUESS** [6,13–15] | Yes, two specific PFTs for northern peatlands: *Sphagnum* moss; flood-tolerant graminoid. | **Scheme:** bucket model. **Hydrological properties:** peat-specific. **Lateral water input:** not considered in this study (but can be considered for site-specific simulations). **Lateral water loss from peatland**: occurs when the volumetric ice fraction of the uppermost acrotelm layer (top 10 cm of peat) <0.7 and determined by the WTP. **Ponding on the surface:** no. **Microtopography:** not considered. | Yes | **Scheme:** acrotelm-catotelm; **Accumulation:** acrotelm-to-catotelm carbon transfer assumed once acrotelm C density exceeds 7.5 kg C $m^{-2}$ **Decomposition** follows Smith et al.[13] , with reduced decomposition for the fraction of C in the catotelm. Decomposition in bulk CENTURY SOM pools controlled by soil moisture and soil temperature at 25 cm depth. | As in Smith et al.[13]. If available mineral N in the soil cannot meet plant N demand, photosynthesis is reduced and allocation of biomass to fine roots may be increased. |
| **LPJ-GUESS_dynP** [2,16,17] | Yes, five specific PFTs for northern peatlands: moss; graminoid; deciduous low shrub; evergreen low shrub; deciduous high shrub | **Scheme:** bucket model, bottom drainage and water percolation depends on the permeability of peat layers and the saturation limit of mineral soils underneath. **Hydrological properties:** peat-specific. **Lateral water input:** yes, the surface of a peatland is represented by uneven heights of individual patches, water is redistributed from the higher | Yes | **Scheme:** dynamic multilayer; **Accumulation:** annual addition of new layers of litter at the top of the soil column; **Decomposition** controlled by volumetric water content and soil temperature at each | No |

| | | | | | |
|---|---|---|---|---|---|
| | | elevated patches to low depressions through lateral flow.<br>**Lateral water loss from peatland:** occurs in the higher elevated patches where the WTP is above the mean WTP of the landscape, and determined by peat porosity and the difference in WTPs between patches.<br>**Ponding on the surface:** yes, it depends on microtopography. When there are connected low elevated patches (hollows), they could form a small pond. Hollows can store water 20 cm above the surface.<br>**Microtopography:** yes | | layer and the litter composition | |
| **LPX-Bern** [6,15,18–20] | Yes, two specific PFTs for northern peatlands: *Sphagnum* moss;<br>flood-tolerant graminoid | **Scheme:** bucket model.<br>**Hydrological properties:** peat-specific.<br>**Lateral water input:** not considered.<br>**Lateral water loss from peatland:** determined by the WTP, occurs when the fractional ice content of the uppermost layer is less than 0.05 and the snow depth is less than 10mm.<br>**Ponding on the surface:** no.<br>**Microtopography:** not considered. | Yes | **Scheme:** acrotelm-catotelm;<br>**Accumulation:** acrotelm-to-catotelm carbon transfer and catotelm-to-acrotelm C transfer (under dry climate conditions);<br>**Decomposition** controlled by WTP and soil temperature. | If plant N uptake cannot meet N demand, NPP is reduced proportionally. |

| | | | | | |
|---|---|---|---|---|---|
| **LPJ-MPI**[5] | Yes, two specific PFTs for northern peatlands: *Sphagnum* moss; flood-tolerant graminoid. Non-peatland PFTs not prohibited, but experience inundation stress | **Scheme:** bucket model. **Hydrological properties:** no specific properties for peat. **Lateral water input:** not considered. **Lateral water loss from peatland:** not considered. **Ponding on the surface:** no. **Microtopography:** not considered. | Yes | **Scheme:** acrotelm-catotelm; **Accumulation:** acrotelm-to-catotelm carbon transfer; **Decomposition** controlled by WTP and soil temperature. | No |

**Table S2.** Representation of soil thermal dynamics of participating models

| Model | Soil thermal scheme | Depth (m) | Moss insulation | Organic soil insulation | Snow scheme | Permafrost/Freezing-thawing cycle |
|---|---|---|---|---|---|---|
| **ORCHIDEE-PEAT**[21] | One-dimensional Fouriers solution | 48 | No | Soil organic carbon (derived from NCSCD and HWSD soil organic carbon map) lowers thermal conductivity and increases heat capacity | 3-layers snow. Energy and water budgets inside the snowpack are resolved, thawing and refreezing of liquid water are accounted for. | Yes |
| **LPJ-GUESS**[6] | Crank-Nicolson finite difference heat diffusion | 48 (1.5 m + 46.5 m padding layers) | No | Yes. Peat layers have specific soil thermal conductivities and heat capacities. | Single-layer snow | Yes |
| **LPJ-GUESS_dynP**[2,6,16,17] | Crank-Nicolson finite difference heat diffusion | 48 | No | Yes. Peat layers have specific soil thermal conductivities and heat capacities | Single-layer snow | Yes |
| **LPX-Bern**[6] | Crank-Nicolson finite difference heat diffusion | 10 | No | No | Single-layer snow | Yes |
| **LPJ-MPI**[22] | Heat diffusion/conduction are not simulated. Soil temperature follows the surface air temperature cycle with a damped oscillation about a common mean, and a temporal lag. | No | No | No | No | No |

**Table S3.** Representation of peatland $CH_4$ production, oxidation and transport of participating models

| Model | $CH_4$ production | $CH_4$ oxidation | $CH_4$ Diffusion | Plant transport | Ebullition |
|---|---|---|---|---|---|
| **ORCHIDEE-PEAT Here use an offline $CH_4$ model developed by Walter et al.**[23,24] | **Substrate:** NPP, which is assumed to be a measure for substrate availability (only fresh organic matter is a suitable substrate for methanogenes). **$CH_4$ production:** a function of the soil temperature and the NPP | $CH_4$ oxidation takes place in soil layers above the water table. Follows the Michaelis-Menten equation and is a function of $CH_4$ concentration and temperature | The Crank-Nicolson numerical scheme. | Proportional to the methane concentration in the soil, affected by density, the growing state (a function of soil temperature at a depth of 50 cm) and the rooting depth of aerenchymatous plants | When the $CH_4$ concentration in a layer exceeds a threshold concentration which is significantly lower than the saturation concentration, the excess $CH_4$ is added into the atmosphere or the lowest unsaturated soil layer depending on the water table depth. |
| **LPJ-GUESS**[25] | **Substrate:** decomposed soil carbon. **$CH_4$ production:** a portion of heterotrophic respiration, affected by temperature and the degree of anoxia. | A function of $CH_4$ concentration and $O_2$ concentration | The Crank-Nicolson numerical scheme. | Follows a concentration gradient between the soil and the atmosphere, affected by the abundance, biomass, phenology and the rooting depth of aerenchymatous plants | $CH_4$ in excess of its maximum solubility escapes to the atmosphere immediately. |
| **LPJ-GUESS_dynP** [2,16,17] | **Substrate**: decomposed soil carbon. **$CH_4$ production**: a portion of heterotrophic respiration, affected by temperature and the degree of anoxia. | A function of $CH_4$ concentration and $O_2$ concentration. | $CH_4$ transport mechanisms are not implemented, instead all the $CH_4$ concentration is directly emitted to the atmosphere after oxidation annually. | | |

| | | | | | |
|---|---|---|---|---|---|
| **LPX-Bern**[6] | **Substrate:** root exudates and decomposed soil carbon.<br>**$CH_4$ production:** a portion of heterotrophic respiration, affected by the degree of anoxia. | A function of $CH_4$ concentration and $O_2$ concentration | The Crank-Nicolson numerical scheme. | Follow a concentration gradient between the soil and the atmosphere, affected by the abundance, biomass, phenology and the rooting depth of aerenchymatous plants | An ebullition event is triggered when the partial pressures of $N_2$, $CO_2$ and $CH_4$ exceed atmospheric and hydrostatic pressure. Gases involved in the event escape to the atmosphere immediately. |
| **LPJ-MPI** [23,24] | **Substrate:** decomposed soil carbon.<br>**$CH_4$ production:** a portion of heterotrophic respiration, affected by temperature and the degree of anoxia | $CH_4$ oxidation takes place in soil layers above the water table.<br>A function of $CH_4$ concentration and temperature | The Crank-Nicolson numerical scheme. | Proportional to the methane concentration in the soil, affected by density, the growing state (a function of the LAI) and the rooting depth of aerenchymatous plants | When the $CH_4$ concentration in a layer exceeds a threshold concentration which is significantly lower than the saturation concentration, the excess $CH_4$ is added into the lowest unsaturated soil layer. |

**Table S4.** Available simulations from ISIMIP2b[7], six land surface models (CLM45, LPJ-GUESS, LPJmL, ORCHIDEE-MICT, VEGAS, VISIT) were forced by climate forcing data from four different GCMs (GFDL-ESM2M, HadGEM2-ES, IPSL-CM5A-LR, MIROC5), under two different greenhouse gas concentration pathways (RCP2.6 and RCP8.5) and future land use was held constant at 2005 levels.

| | CLM45 | LPJ-GUESS | LPJmL | ORCHIDEE-MICT | VEGAS | VISIT |
|---|---|---|---|---|---|---|
| **Historical** | | | | | | |
| GFDL-ESM2M | | 1861-2005 | 1861-2005 | 1861-2005 | | 1861-2005 |
| HadGEM2-ES | | 1861-2005 | 1861-2005 | 1861-2005 | | 1861-2005 |
| IPSL-CM5A-LR | | 1861-2005 | 1861-2005 | 1861-2005 | 1861-2005 | 1861-2005 |
| MIROC5 | | 1861-2005 | 1861-2005 | 1861-2005 | | 1861-2005 |
| **RCP2.6** | | | | | | |
| GFDL-ESM2M | 2006-2099 | 2006-2099 | 2006-2099 | 2006-2099 | | 2006-2099 |
| HadGEM2-ES | **2006-2299** | **2006-2299** | **2006-2299** | 2006-2099 | | **2006-2299** |
| IPSL-CM5A-LR | 2006-2099 | **2006-2299** | **2006-2299** | **2006-2299** | **2006-2299** | **2006-2299** |
| MIROC5 | 2006-2099 | **2006-2299** | **2006-2299** | 2006-2099 | | **2006-2299** |
| **RCP8.5** | | | | | | |
| GFDL-ESM2M | 2006-2099 | 2006-2099 | 2006-2099 | 2006-2099 | | 2006-2099 |
| HadGEM2-ES | 2006-2099 | 2006-2099 | 2006-2099 | 2006-2099 | | 2006-2099 |
| IPSL-CM5A-LR | 2006-2099 | 2006-2099 | 2006-2099 | 2006-2099 | | 2006-2099 |
| MIROC5 | 2006-2099 | 2006-2099 | 2006-2099 | 2006-2099 | | 2006-2099 |

**Supplemental References**


1. Qiu, C., Zhu, D., Ciais, P., Guenet, B., Peng, S., Krinner, G., Tootchi, A., Ducharne, A., and Hastie, A. (2019). Modelling northern peatland area and carbon dynamics since the Holocene with the ORCHIDEE-PEAT land surface model (SVN r5488). Geosci. Model Dev. *12*, 2961–2982.
2. Chaudhary, N., Miller, P.A., and Smith, B. (2017). Modelling Holocene peatland dynamics with an individual-based dynamic vegetation model. Biogeosciences *14*, 2571–2596.
3. Rosnay, P. De, and Polcher, J. (2002). Impact of a physically based soil water flow and soil-plant interaction representation for modeling large-scale land surface processes. J. Geophys. Res. *107*, 4118.
4. Qiu, C., Zhu, D., Ciais, P., Guenet, B., Krinner, G., Peng, S., Aurela, M., Bernhofer, C., Brümmer, C., Bret-Harte, S., et al. (2018). ORCHIDEE-PEAT (revision 4596), a model for northern peatland CO2, water, and energy fluxes on daily to annual scales. Geosci. Model Dev. *11*, 497–519.
5. Kleinen, T., Brovkin, V., and Schuldt, R.J. (2012). A dynamic model of wetland extent and peat accumulation: Results for the Holocene. Biogeosciences *9*, 235–248.
6. Wania, R., Ross, I., and Prentice, I.C. (2009). Integrating peatlands and permafrost into a dynamic global vegetation model: 1. Evaluation and sensitivity of physical land surface processes. Global Biogeochem. Cycles *23*, 1–19.
7. Frieler, K., Lange, S., Piontek, F., Reyer, C.P.O., Schewe, J., Warszawski, L., Zhao, F., Chini, L., Denvil, S., and Emanuel, K. (2017). Assessing the impacts of 1.5 C global warming–simulation protocol of the Inter-Sectoral Impact Model Intercomparison Project (ISIMIP2b). Geosci. Model Dev. *10*, 4321–4345.
8. Hugelius, G., Loisel, J., Chadburn, S., Jackson, R.B., Jones, M.C., MacDonald, G.M., Marushchak, M.E., Olefeldt, D., Packalen, M., Siewert, M.B., et al. (2020). Large stocks of peatland carbon and nitrogen are vulnerable to permafrost thaw. Proc. Natl. Acad. Sci. *117*, 20438–20446.
9. Batjes, N.H. (2016). Harmonized soil property values for broad-scale modelling (WISE30sec) with estimates of global soil carbon stocks. Geoderma *269*, 61–68.
10. Xu, J., Morris, P.J., Liu, J., and Holden, J. (2018). PEATMAP: Refining estimates of global peatland distribution based on a meta-analysis. Catena *160*, 134–140.
11. Treat, C.C., Bloom, A.A., and Marushchak, M.E. (2018). Nongrowing season methane emissions–a significant component of annual emissions across northern ecosystems. Global Change Biol. *24*, 3331–3343.
12. Brown, J., Ferrians, O., Heginbottom, J.A., and Melnikov, E.S. (2002). Circum-Arctic map of permafrost and ground-ice conditions, Version 2. Boulder, Colorado USA. NSIDC: National Snow and Ice Data Center. (last access: October, 2020).
13. Smith, B., Warlind, D., Arneth, A., Hickler, T., Leadley, P., Siltberg, J., and Zaehle, S. (2014). Implications of incorporating N cycling and N limitations on primary production in an individual-based dynamic vegetation model. Biogeosciences *11*, 2027–2054.
14. McGuire, A.D., Christensen, T.R., Hayes, D., Heroult, A., Euskirchen, E., Kimball, J.S., Koven, C., Lafleur, P., Miller, P.A., Oechel, W., et al. (2012). An

assessment of the carbon balance of Arctic tundra: comparisons among observations, process models, and atmospheric inversions. Biogeosciences *9*, 3185–3204.
15. Wania, R., Ross, I., and Prentice, I.C. (2009). Integrating peatlands and permafrost into a dynamic global vegetation model: 2. Evaluation and sensitivity of vegetation and carbon cycle processes. Global Biogeochem. Cycles *23*, 1–15.
16. Chaudhary, N., Miller, P.A., and Smith, B. (2017). Modelling past, present and future peatland carbon accumulation across the pan-Arctic region. Biogeosciences *14*, 4023.
17. Chaudhary, N., Westermann, S., Lamba, S., Shurpali, N., Sannel, A.B.K., Schurgers, G., Miller, P.A., and Smith, B. (2020). Modelling past and future peatland carbon dynamics across the pan-Arctic. Global Change Biol. *26*, 4119–4133.
18. Stocker, B.D., Spahni, R., and Joos, F. (2014). DYPTOP: A cost-efficient TOPMODEL implementation to simulate sub-grid spatio-temporal dynamics of global wetlands and peatlands. Geosci. Model Dev. *7*, 3089–3110.
19. Spahni, R., Joos, F., Stocker, B.D., Steinacher, M., and Yu, Z.C. (2013). Transient simulations of the carbon and nitrogen dynamics in northern peatlands: From the Last Glacial Maximum to the 21st century. Clim. Past *9*, 1287–1308.
20. Müller, J., and Joos, F. (2020). Global peatland area and carbon dynamics from the Last Glacial Maximum to the present – a process-based model investigation. Biogeosciences *17*, 5285–5308.
21. Guimberteau, M., Zhu, D., Maignan, F., Huang, Y., Yue, C., Dantec-Nédélec, S., Ottlé, C., Jornet-Puig, A., Bastos, A., Laurent, P., et al. (2018). ORCHIDEE-MICT (v8. 4.1), a land surface model for the high latitudes: model description and validation. Geosci. Model Dev. *11*, 121–163.
22. Sitch, S., Smith, B., Prentice, I.C., Arneth, A., Bondeau, A., Cramer, W., Kaplan, J.O., Levis, S., Lucht, W., Sykes, M.T., et al. (2003). Evaluation of ecosystem dynamics, plant geography and terrestrial carbon cycling in the LPJ dynamic global vegetation model. Global Change Biol. *9*, 161–185.
23. Walter, B.P., and Heimann, M. (2000). A process-based, climate-sensitive model to derive methane emissions from natural wetlands: Application to five wetland sites, sensitivity to model parameters, and climate. Global Biogeochem. Cycles *14*, 745–765.
24. Walter, B.P., Heimann, M., and Matthews, E. (2001). Modeling modern methane emissions from natural wetlands: 1. Model description and results. J. Geophys. Res. Atmos. *106*, 34189–34206.
25. Wania, R., Ross, I., and Prentice, I.C. (2010). Implementation and evaluation of a new methane model within a dynamic global vegetation model: LPJ-WHyMe v1.3.1. Geosci. Model Dev. *3*, 565–584.